JCI The Journal of Clinical Investigation

Sec13 promotes oligodendrocyte differentiation and myelin repair through autocrine pleiotrophin signaling

Zhixiong Liu, … , Zhanxiang Wang, Liang Zhang

J Clin Invest. 2022. https://doi.org/10.1172/JCI155096.

Research In-Press Preview Cell biology Neuroscience

Graphical abstract

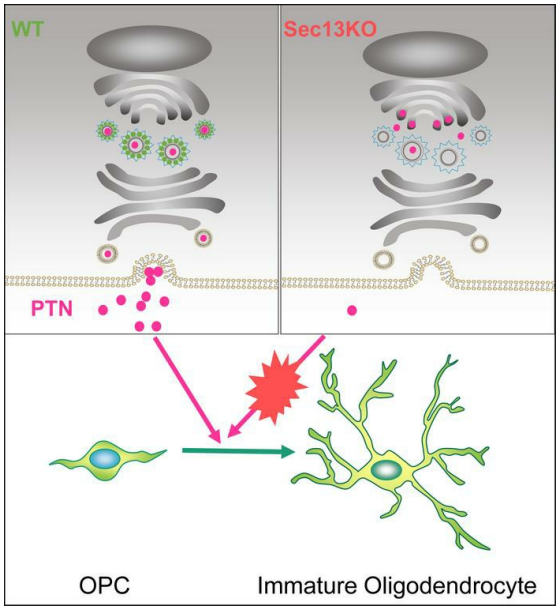

Sec13 promotes oligodendrocyte differentiation and myelin repair through autocrine pleiotrophin signaling

Zhixiong Liu[1,2,3,5], Minbiao Yan[1,2,3,5], Wanying Lei[1,2,3,5], Rencai Jiang[3], Wenxiu Dai[3], Jialin Chen[3], Chaomeng Wang[3], Li Li[3], Mei Wu[3], Ximing Nian[3], Daopeng Li[3], Di Sun[3], Xiaoqi Lv[3], Chaoying Wang[3], Changchuan Xie[3], Luming Yao[3], Caiming Wu[3], Jin Hu[3], Naian Xiao[4], Wei Mo[1,2,3], Zhanxiang Wang[1,2*], and Liang Zhang[1,2,3*]

[1]Department of Neuroscience, Institute of Neurosurgery, and Department of Neurosurgery, the First Affiliated Hospital, State Key Laboratory of Cellular Stress Biology, School of Medicine, Xiamen University, Xiamen, Fujian 361102, China

[2]Xiamen Key Laboratory of Brain Center, the First Affiliated Hospital, Xiamen University, Xiamen, Fujian 361102, China

[3]School of Life Sciences, Innovation Center for Cell Signaling Network, Xiamen University, Xiamen, Fujian 361102, China

[4]Department of Neurology, the First Affiliated Hospital, Xiamen University, Xiamen, Fujian 361003, China

[5]These authors contributed equally

*Correspondence: wangzx@xmu.edu.cn (Z.W.), lzhangxmu@xmu.edu.cn (L.Z.)

Abstract

Dysfunction of protein trafficking has been intensively associated with neurological diseases, including neurodegeneration, but whether and how protein transport contributes to oligodendrocyte maturation and myelin repair in white matter injury remains unclear. ER-to-Golgi trafficking of newly synthesized proteins is mediated by the coat protein complex II (COPII) complex. Here we demonstrate that COPII component Sec13 is essential for oligodendrocyte differentiation and postnatal myelination. Ablation of Sec13 in oligodendrocyte lineage prevented OPC differentiation and inhibited myelination and remyelination after demyelinating injury in central nervous system (CNS), while improving protein traffic by tauroursodeoxycholic acid (TUDCA) or ectopic expression of COPII components accelerated myelination. COPII components were upregulated in oligodendrocyte lineage cells after demyelinating injury. Loss of Sec13 altered the secretome of oligodendrocytes and inhibited the secretion of PTN, which was identified to function as an autocrine factor to promote oligodendrocyte differentiation and myelin repair. These data suggest that Sec13-dependent protein transport is essential for oligodendrocyte differentiation and Sec13-mediated PTN autocrine signaling is required for proper myelination and remyelination.

Introduction

Myelination in the central nervous system (CNS) by oligodendrocytes (OLs) is essential for rapid impulse conduction and normal brain function (1, 2). Disrupted myelin repair impairs nerve conduction and contributes to neurological dysfunction, axon degeneration and disease progression, such as multiple sclerosis (MS) and leukodystrophies (3). Oligodendrocyte progenitor cells (OPCs) are present in demyelinated regions of MS patients and there is evidence of impaired oligodendrocyte differentiation (4). Therefore, understanding how OL differentiation and remyelination is regulated has implications for proper brain functions and therapy of demyelinating diseases.

Disrupted protein transport and abnormal protein aggregation have been frequently observed and studied in neurological diseases (5). Trafficking of trans-membrane and soluble proteins from the endoplasmic reticulum (ER) to the Golgi organelle is mediated by COPII (6). COPII is composed of five core components, including a small GTPase SAR1 and two cytosolic protein complexes, Sec23-Sec24 and Sec13-Sec31 (6). Dysregulation of COPII components has been reported to inhibit protein secretion and affect cell differentiation, function and homeostasis (7-12). Increasing evidence has indicated the connections between COPII components and human neurological disorders. Sec24B variants induce neural tube defects (13). Mutant Sec31A causes a severe neurological syndrome (14). During OL differentiation, OLs undergo remarkable process extension and membrane expansion, which is accompanied with a large

amount of protein trafficking (15). However, a comprehensive understanding of the physiological function and the underlying mechanism of COPII components in oligodendrocyte differentiation and myelination is missing.

Both extrinsic environmental signals and intrinsic signaling pathways play important roles in regulating OL differentiation (16). Among extracellular cues, the majority of them are paracrine factors, released from other cells, such as astrocytes (17, 18). Much less is known about whether oligodendrocyte differentiation is also regulated by autocrine signaling. Here, we found that COPII components were upregulated after demyelinating injury. Ectopic expression of these components promoted oligodendrocyte differentiation, whereas knockdown of these components impaired myelin gene transcription. Ablation of COPII component Sec13 prevented OPC differentiation and myelination by inhibiting PTN secretion. Mechanistically, the autocrine PTN signaling promotes OL maturation by binding to PTPRZ receptor and activating p190RhoGAP signaling. Moreover, exogenous expression of PTN accelerated remyelination after demyelination injury. These findings suggest that COPII component Sec13 is required for oligodendrocyte differentiation and Sec13-mediated autocrine PTN signaling plays an important role in CNS myelination.

Results

COPII complex is implicated in remyelination after demyelination

OPCs exist in adult mouse CNS and can differentiate into mature OLs to mediate adult myelinogenesis, which is important for remyelination following demyelinating injury (19, 20). Focal injection of lysolecithin (LPC) in the white matter causes acute demyelinating injury followed by myelin regeneration (21). We found that expression of COPII component, Sec13 and Sec31A, was hardly detectable in non-lesion regions of adult spinal white matter, and focal injection of PBS did not affect their expression, however their expression was significantly upregulated following demyelination and it was substantially expressed in oligodendrocyte lineage as indicated by Olig2-expressing cells (Figure 1, A-D), indicating that protein trafficking mediated by COPII may play important roles during remyelination process. Similar findings were also observed in Ethidium bromide (EB)-induced demyelination assay (Supplemental Figure 1, A and B). We further analyzed the expression patterns of COPII components during oligodendrocyte differentiation. Sec13, Sec23B, Sar1A, Sar1B and Sec31A were upregulated in response to differentiation cues in vitro (Figure 1E and Supplemental Figure 1C). These data indicate that COPII-mediated protein transport might be important for remyelination in CNS. Therefore, we examined that whether TUDCA, which is a chemical chaperone and was shown to ameliorate protein transport (22, 23), could accelerate remyelination after LPC-induced demyelinating injury. Surprisingly, at 10 days post-lesion (dpl), myelin repair was significantly accelerated in corpus callosum region of mice treated with 500 mg kg^{-1} TUDCA once a day for eleven

days as indicated with MBP (myelin basic protein) staining (Figure 2, A-C). Although the number of PDGFRα$^+$ OPCs in lesion site was slightly decreased after TUDCA treatment (Supplemental Figure 2, A-B), lesion size or the number of Olig2$^+$ oligodendrocytes in lesion site was not affected (Supplemental Figure 2, C-E). In addition, treatment with ER-Golgi trafficking inhibitor Brefeldin A (BFA) strongly inhibited expression of myelin genes (Figure 2, D-F). Collectively, these findings indicate that COPII-mediated protein transport is implicated in oligodendrocyte differentiation and remyelination.

COPII component Sec13 is required for myelination in CNS

To further gain insights into the functions of COPII during OL development, we respectively attenuated their expression in primary rat OPCs using small interfering RNAs (siRNAs) (Supplemental Figure 3A). Knockdown of COPII components individually inhibited expression of myelin-associated genes, including *Cnp* (2',3'-cyclic nucleotide 3'-phosphodiesterase) and *Plp1* (proteolipid protein) (Supplemental Figure 3B), suggesting that COPII is critical for proper OL differentiation in vitro. Sec13 needs to cooperate with Sec31 to promote COPII vesicle budding and protein secretion (24, 25). In agreement with this, co-transfection of Sec13 and Sec31A, but not Sec13 or Sec31A alone, promoted myelin gene transcription and CNP protein expression (Supplemental Figure 3, C-D). Unlike other COPII components, there is only one Sec13 isoform and knockdown of Sec13 impairs cell differentiation, we therefore focus on Sec13 function in OL development. Sec13 was strongly expressed in CC1$^+$

oligodendrocyte, but weakly in PDGFRα^+ OPCs in the P14 corpus callosum (Figure 3A). The proportions of CC1$^+$ among Sec13$^+$ cells in the corpus callosum at P14 are 66%, suggesting that Sec13 is largely restricted to differentiating OLs in the OL lineage (Figure 3B). Sec13 expression was also observed in NeuN$^+$ neurons in the cortex adjacent to corpus callosum, but was hardly detectable in glial fibrillary acidic protein (GFAP)$^+$ astrocytes, or IBA1$^+$microglia in the corpus callosum at P14 (Supplemental Figure 3E). Similarly, other COPII components Sar1B and Sec23A were also detected in Olig2$^+$ oligodendrocytes and NeuN$^+$ neurons, but not in GFAP$^+$ astrocytes, or IBA1$^+$microglia (Supplemental Figure 4, A-B). Consistent with previous observations (26), Sec13 is primarily located at the ER exit site (ERES) where it colocalizes with Sec24A in early differentiating immature oligodendrocytes (Supplemental Figure 4C). To assess the role of Sec13 in oligodendrocyte development in vivo, we crossed Sec13 hypomorphic mice with FLPe-expressing transgenic mice to remove NEO cassette (Supplemental Figure 4, D-E) (27). The resulting Sec13$^{flox/flox}$ mice show comparable expression level with wild type mice (Supplemental Figure 4F). We then selectively deleted Sec13 in the oligodendrocyte lineage by crossing Sec13$^{flox/flox}$ mice with an Olig1-Cre line that directing Cre expression in the oligodendrocyte lineage cells (28), including OPCs and mature myelinating oligodendrocytes in the CNS. Sec13 protein expression in Olig2$^+$ oligodendrocytes was substantially reduced in the spinal cord and corpus callosum of *Sec13* conditional knockout mice (*Sec13* $^{flox/flox}$; *Olig1-Cre*$^{+/-}$, *Sec13*cKO) at postnatal day (P) 14 (Supplemental Figure 5, A-D). In contrast, Sec13 expression was not affected in NeuN$^+$ neurons (Supplemental Figure 5, E-F). The

160 resulting *Sec13*cKO mutant mice were born at Mendelian ratio and appeared to be
161 normal at birth, but developed severe tremor and seizures, reminiscent of myelin-
162 deficient mice, and died at postnatal week 2 in contrast to the normal life span of wild-
163 type and heterozygotes (Figure 3C). The myelinating optic nerve from *Sec13*cKO at
164 P12 was translucent compared to the control, indicating severe hypomyelination
165 (Figure 3D). Indeed, the expression of myelin markers such as MBP (myelin basic
166 protein) and *Plp* was significantly diminished in the spinal cord and corpus callosum of
167 mutant mice at P14 (Figure 3, E-H, and Supplemental Figure 6A). The extent of
168 myelination was also assessed by staining with FluoroMyelin and a decrease of
169 myelination in the corpus callosum of mutant mice at P14 was observed (Supplemental
170 Figure 6B). Myelination deficits were further confirmed by electron microscopy.
171 Myelinated axons were hardly detectable in the optic nerve or spinal cord of mutant
172 mice at P14, in contrast to the large number of myelinated axons that were observed
173 in control mice (Figure 3I). The thickness of myelin sheaths around axons assessed
174 by g-ratios were substantially reduced in mutant mice (Figure 3J). Together, these data
175 suggest that COPII component Sec13 is required for CNS myelination.

176 Since Sec31A cooperates with Sec13 to promoted myelin gene transcription and
177 was upregulated upon LPC injury, we therefore tested the function of Sec31A in
178 developmental myelination. Mice were injected with ASO (modified anti-sense oligos)
179 against Sec31A mRNA at P3 and harvested at P14. The MBP signal intensity was
180 remarkably decreased in the brain of ASO-Sec31A-injected mice compared to control.
181 (Supplemental Figure 6, C-D).

182

183 **Sec13 is required for OPC differentiation**

184 The hypomyelination phenotype detected in Sec13 mutant mice could be due to
185 arrested OPC maturation. To test this hypothesis, OPC and oligodendrocyte numbers
186 were analyzed. In contrast with the markedly reduction of $CC1^+$ oligodendrocytes, the
187 total numbers of PDGFRα^+ OPCs were comparable between control and *Sec13*cKO
188 mutants (Figure 4, A-D). Loss of Sec13 did not appear to change the number of $Olig2^+$
189 oligodendrocytes (Figure 4, E-F). We did not detect any significant increase of
190 apoptotic cells by TUNEL assay (Figure 4, G-H). Meanwhile, the Sec13 mutants did
191 not exhibit significant alteration of astrocytes, neurons or axons identified by GFAP,
192 NeuN and NF200 staining (Supplemental Figure 7, A-B). These data suggest that
193 ablation of Sec13 prevents OPCs from differentiation. To further determine whether
194 defects in the OL maturation in *Sec13*cKO animals are cell autonomous due to *Sec13*
195 deletion, we purified OPCs by immunopanning from the neonatal brain for in vitro
196 studies. Loss of Sec13 resulted in a significant decrease in the number of MBP^+ or
197 CNP^+ oligodendrocytes after triiodothyronine (T3) induction, whereas the cells
198 remained a PDGFRα-expressing state (Figure 4, I-J, and Supplemental Figure 7, C-
199 D). Consistently, myelin associated gene transcripts was also significantly inhibited
200 (Supplemental Figure 7E). In addition, reduction of Sec13 with siRNA-mediated
201 knockdown in rat OPCs resulted in a similar decrease in the number of MBP^+
202 oligodendrocytes. In contrast, control OPCs readily differentiated into MBP^+ OLs
203 (Supplemental Figure 7, F-H). Furthermore, reintroduction of siRNA-resistant Sec13

could rescue the defects in myelin gene expression (Supplemental Figure 7I). To further examine the effects of Sec13 inactivation on OPC differentiation during early postnatal development in a time-controlled manner, we generated OPC-inducible *Sec13* mutants by crossing *Sec13* $^{flox/flox}$ mice with *PDGFRα-CreERT* mice and inducing recombination of Sec13 in OPCs at P3 by tamoxifen administration (Supplemental Figure 8A). Effective depletion of Sec13 in Olig2^{+} oligodendrocytes was observed (Supplemental Figure 8, B-C) and expression of MBP in *PDGFRα-CreERT*: *Sec13*$^{flox/flox}$ mutants (*Sec13*-iKO) mice was reduced compared with control littermates at P12 (Supplemental Figure 8, D-E). Together, these findings suggest that Sec13 is required for OPC differentiation.

Sec13 is critical for adult remyelination after demyelination

Given the essential role of Sec13 in developmental myelination, we hypothesized that Sec13 was required for remyelination after injury. We administered tamoxifen garage prior to LPC injection in control (*Sec13* $^{flox/flox}$) and *Sec13*iKO (*NG2-CreERT*: *Sec13* $^{flox/flox}$) 8-week-old mice (Figure 5A), which induced effective depletion of Sec13 in Olig2^{+} oligodendrocytes (Figure 5, B-C). At 14 dpl and 21 dpl, MBP expression was substantially reduced in the corpus callosum and spinal cord of *Sec13*iKO mice compared to control (Figure 5, D-G), whereas the lesion area was similar between control and iKO mice (Figure 5F and Supplemental Figure 9A). Consistent with these findings, fewer CC1^{+} differentiating oligodendrocytes were detected in the lesions of Sec13iKO corpus callosum and spinal cord than control (Figure 5, H-I and

Supplemental Figure 9, B-C). In contrast, depletion of Sec13 did not appear to impair the recruitment of PDGFRα^+ OPCs or their proliferation (Supplemental Figure 9, D-E) (29). Quantification of Olig2$^+$ or PDGFRα^+ cells, IBA1$^+$ microglia or GFAP$^+$ astrocytes indicated that loss of Sec13 did not alter their formation or recruitment (Supplemental Figure 9F). Ultrastructural analysis by electron microscopy further indicated that there were far fewer myelinated axons in the lesions of *Sec13*iKO mice than in control (Figure 5J). The proportions of myelinating axons and the thickness of myelin sheaths indicated as g-ratio were significantly decreased in *Sec13*iKO mice (Figure 5, K-L). Notably, focal injection of lentivirus expressing Sec13 can restore the remyelination in *Sec13*iKO mice (Supplemental Figure 9, G-H). Thus, these data suggest that Sec13 is crucial for the OL remyelination process after white matter injury.

Ablation of Sec13 does not affect nucleocytoplasmic transport and mTOR signaling

Sec13 is a multifunctional protein. In addition to its major function in the COPII complex, Sec13 also plays a role in the nuclear pore complex (30). Therefore, we decided to determine whether the hypomyelination phenotype was caused by defects in nuclear transport. Staining with mAb414, a diagnostic NPC assembly marker that detects a subset of FG-Nups (31), showed similar staining intensity and structure between control and mutant Olig2$^+$ oligodendrocytes from spinal cord or primary cells (Supplemental Figure 10, A-B). Moreover, the levels of several nucleoporins were similar between control and mutant spinal cord protein extracts, indicating that

absence of Sec13 did not appear to change proportions of other nucleoporins (Supplemental Figure 10C). Optic nerves from *Sec13*cKO mice also showed absence of nuclear-envelope alteration or NPC clustering by electron microscopy (Supplemental Figure 10D). As NPCs are critical for regulating the passage of molecules between the nucleus and the cytoplasm, we therefore investigated whether loss of Sec13 would affect general nucleocytoplasmic transport. Oligodendrocyte cell line Oli-neu cells were transfected with tdTomato containing a Nuclear Localization Signal (NLS) or Nuclear Export Signal (NES) (31), and no significant difference in the localization of tdTomato signals were observed (Supplemental Figure 10E). To assess whether Sec13 depletion affected the transport of mRNAs, oligo-dT *in situ* hybridization was performed (32). No significant difference in the intracellular distribution of poly $(A)^+$ RNA was observed between control and Sec13-knockdown Oli-neu cells (Supplemental Figure 10F). Collectively, these data suggest that depletion of Sec13 does not affect global NPC assembly or function in oligodendrocytes.

In addition, Sec13 also belongs to the GATOR2 complex, a positive regulator of the mTORC1 pathway (33). We thus tested the phosphorylation state of mTOR signaling downstream S6 protein. Knockdown of Sec13 in Oli-neu cells did not significantly inhibit the amino acid-induced activation of mTORC1, as detected by the phosphorylation state of S6 (Supplemental Figure 10, G-H). Thus, Sec13 may not regulate oligodendrocytes differentiation through major changes in mTOR signaling. Overall, these results suggest that Sec13 does not regulate oligodendrocyte differentiation through major alterations in nucleocytoplasmic transport or mTOR

signaling.

Sec13 regulates oligodendrocyte secretome

Sec13 is an essential component of COPII vesicles and is involved in protein traffic from ER to Golgi (24, 25, 34). Loss of COPII components have been reported to cause expanded ER due to intracellular protein accumulation (8, 34, 35). To explore the cause of the arrested OL differentiation in *Sec13*cKO mice, transmission electron microscopy was performed and revealed that ablation of Sec13 cause ER distension in spinal cord from mutant mice (Figure 6, A-B). Meanwhile, we further found a concomitant decrease of Sec24A and Sec31A expression in mouse OPCs isolated from *Sec13*cKO mice (Figure 6C), which is consistent with previous results from HeLa cells (36). The significant down-regulation of Sec31A was confirmed by immunostaining results of mouse primary OPCs (Supplemental Figure 11A). Interestingly, a compensatory upregulation was observed in RNA levels of a subset of COPII components (Supplemental Figure 11B). Retention of excessive amounts of protein in ER can lead to activation of unfolded protein response (UPR) pathway (12). We therefore examined the expression of markers associated with UPR activation. Unexpectedly, the levels of phosphorylated eIF2α, a substrate of PERK (37), was not significantly increased by depletion of Sec13 (Figure 6D). Similarly, the levels of BIP, ATF4, ATF6 and CHOP, a transcription factor that promotes ER stress-mediated apoptosis (38), also remain unchanged in rat OPCs and spinal cord lysates after ablation of Sec13 (Figure 6E and Supplemental Figure 11C). Soluble proteins are packaged into COPII complex and delivered to the Golgi for further processing. In addition, several COPII components

have been shown to regulate cell differentiation, chondrogenesis and tumor metastasis by mediating secretion of relevant proteins (7, 8, 11). We thus investigated whether proteins secreted by OL would autonomously promote OL differentiation and loss of Sec13 impairs the secretion of these proteins. First, we assessed the ability of the conditioned medium (CM) from differentiating immature oligodendrocytes to promote OL differentiation. Compared to plain DMEM/F-12 medium, CM significantly increased myelin gene transcription, indicating differentiating immature oligodendrocytes may regulate self-differentiation by autocrine signaling (Figure 6F). In contrast, CM from microglia or astrocytes showed much weaker activities to affect transcription of myelin genes (Supplemental Figure 11D). To better understand the underlying mechanism by which Sec13 regulates OL differentiation and decipher the potential autocrine factors, we compared the secretome of OPCs and differentiating immature oligodendrocytes in the absence or presence of siRNA against Sec13. There was a global increase in secretion of proteins upon differentiation (Figure 6G), whereas knockdown of Sec13 strongly inhibited protein secretion (Figure 6H and Supplemental Table1). 47% (110/236) proteins which were originally upregulated in secretome upon differentiation showed less abundance in CM from *Sec13*-knockdown differentiating immature oligodendrocytes (Figure 6I). GO (Gene Ontology) analysis revealed that proteins involved in cell adhesion and protein folding were most significantly affected by knockdown of Sec13 (Figure 6J). Together, these data suggest that Sec13 regulates the secretome of oligodendrocyte.

PTN promotes oligodendrocyte differentiation via autocrine signaling

To uncover the central mediators of the secretome that promote OL differentiation, we then focused on those factors which have reduced abundance after knockdown of Sec13. We functionally tested five candidates (pleiotrophin (PTN), leukemia inhibitory factor (LIF), apolipoprotein E (APOE), midkine (MDK), cysteine sulfinic acid decarboxylase (CSAD)) by adding recombinant factors. Among candidates, the addition of PTN, but not other factors, strongly potentiated myelin gene transcription (Figure 7A). In addition, MBP and CNP were induced by PTN at protein levels (Supplemental Figure 12, A-C). Meanwhile, depletion of PTN with anti-PTN antibody impaired the ability of CM to promote myelin gene transcription, indicating that PTN is the central mediators in CM that promote OL differentiation (Supplemental Figure 12D). Knockdown of PTN inhibited myelin gene transcription and CNP expression (Supplemental Figure 12, E-F and Figure 7B), phenocopying *Sec13* knockdown. PTN transcript level was substantially induced upon OL differentiation (Supplemental Figure 12G). Furthermore, in the developing corpus callosum, PTN expression peaked at the perinatal stage P8 in Olig2^{+} oligodendrocyte lineage, just prior to myelination onset (Supplemental Figure 12H). Moreover, upon oligodendrocyte differentiation, PTN concentrates to the ERES as indicated by COPII component Sec24A (Supplemental Figure 12I). Taken together, our data indicate that PTN is highly expressed in differentiating OLs in the OL lineage.

PTN transcript remained unchanged after knockdown of Sec13 (Supplemental Figure 12J), however intracellular accumulation and reduced secretion of PTN were

observed in Sec13-knockdown Oli-neu cell lines (Figure 7C). Furthermore, analysis of PTN cellular distribution by immunofluorescence also demonstrated significant accumulation in the ER of mouse differentiating immature oligodendrocytes from Sec13 mutant, as indicated by ER marker, protein disulfide isomerases (PDI) (Supplemental Figure 13A). BFA disrupts the Golgi apparatus and consequently the delivery of ER-derived COPII vesicles along the secretory pathway (9). Treatment of BFA in differentiating immature oligodendrocytes led to intracellular PTN accumulation (Supplemental Figure 13, B-C). These data suggest that COPII component Sec13-mediated ER-Golgi transport plays a critical role in PTN secretion. To further validate that secreted PTN has a direct effect on OL differentiation, we utilized a PTN mutant (L18&20R), which had mutated signal peptide and could not be secreted to medium (Supplemental Figure 13D). Ectopic expression of PTN, but not PTN mutant, not only stimulated OPCs differentiation into CNP^+ oligodendrocyte (Figure 7, D-E), but also upregulated transcription of myelin genes (Supplemental Figure 13E). Because depletion of Sec13 inhibited OL differentiation and PTN secretion, we hypothesized that the exogenous replenishment of PTN could rescue the developmental defects of OL in Sec13-knockdown cells. By adding PTN to OPCs, we found that PTN significantly increased the number of MBP^+ oligodendrocyte in Sec13-knockdown cells, indicating that PTN mediated Sec13 function in OL differentiation (Figure 7, F-G). Taken together, these data suggest that Sec13 functions as a COPII component to regulates OL differentiation primarily through mediating PTN secretion.

We next examined how PTN regulates OL differentiation. PTN has been reported

to function through several putative receptors, such as protein tyrosine phosphatase receptor type Z1 (PTPRZ1), anaplastic lymphoma receptor tyrosine kinase (ALK), chondroitin sulfate proteoglycan 5 (CSPG5) and syndecan 3 (SDC3) (39, 40). By immunoprecipitation, we found that PTN specifically binds to PTPRZ1 in differentiating immature oligodendrocytes (Figure 7H). PTPRZ1 is a tyrosine phosphatase and is inactivated after binding with PTN (41). Previous studies have shown that PTN-PTPRZ signaling can activate several downstream effectors (42). Here we found that exogenous PTN significantly increased the phosphorylation of p190RhoGAP, but not other reported effectors in OLs (Figure 7I). p190RhoGAP, a GTPase-activating protein (GAP), is phosphorylated at Tyr1105 during OL differentiation and this modification enhances GAP activity, thereby suppressing the Rho-ROCK pathway, resulting in the maturation of oligodendrocytes and myelination (43-45). Moreover, knockdown of p190RhoGAP attenuated the effect of exogenous PTN treatment on myelin gene transcription (Figure 7J). Collectively, these data demonstrate that Sec13-mediated PTN autocrine signaling promote cell differentiation through PTPRZ- p190RhoGAP pathway.

PTN accelerate remyelination after demyelinating injury

Given the PTN function on oligodendrocyte differentiation, we then asked whether PTN played an important role in remyelination after demyelination injury. Although PTN was not previously detected in OL lineage in cuprizone-induced demyelinating model (46), we indeed observed that PTN was upregulated in Olig2-expressing cells upon LPC

injury (Figure 8A). The discrepancy may result from the difference between LPC and cuprizone injury models, since LPC-injection induces acute demyelination compared to cuprizone treatment. By co-injecting lysolecithin lesions with lentivirus expressing shRNA-PTN into spinal cord (Figure 8B), we found that knockdown of PTN significantly impaired remyelination compared to lentivirus expressing scrambled shRNA (Figure 8, C-D and Supplemental Figure 14, A-B), whereas recruitment of $IBA1^+$ cells or lesion area were comparable (Supplemental Figure 14, C-F). Similar results showing decrease in remyelination were also obtained in the corpus callosum of mice injected with lentivirus expressing shRNA-PTN (Supplemental Figure 14, G-I). To further validate the role of PTN in remyelination, we next used retrovirus expressing PTN or mutant PTN in the LPC demyelinating model (Figure 8E). At the 10 days post injury, MBP and *Plp1* expression was significantly increased following RV-PTN administration (Figure 8, F-G and Supplemental Figure 15, A-C). By contrast, ectopic expressing of the mutant PTN (L18&20R), which could not be secreted, could not substantially accelerate remyelination (Figure 8, F-G and Supplemental Figure 15, A-C). Accelerated remyelination was confirmed by electron microscopy of the corpus callosum, which revealed improved axonal ensheathment with increased number of myelinated axons by ectopic expression of PTN (Supplemental Figure 15, D-E). These data demonstrate that PTN is required for remyelination and secreted PTN is able to accelerate remyelination upon white matter injury.

Discussion

Physiological function of COPII in the CNS

During OL differentiation, OLs undergo thousand-fold increase in membrane area and remarkable process extension (15), which is accompanied with a large amount of protein trafficking. Here we investigate expression patterns of COPII components during OL differentiation and hypomyelination phenotype after specifically depleting Sec13 in the OL lineage. At the peak of myelination (P14) in the mouse CNS, COPII components were mainly found in oligodendrocytes and neurons, but were hardly detectable in astrocytes and microglia, which is conceivable given the requirement of oligodendrocytes and neurons for protein trafficking. Moreover, improving protein transport with TUDCA or inhibiting it with BFA can both significantly affect OL differentiation. It is noteworthy that Sec13 and another COPII protein Sec31A are up-regulated upon LPC-induced demyelination injury, indicating that protein trafficking is highly required during myelin repair. Whether expression levels of other COPII components will change responding to demyelination injury remains unanswered. The COPII complex captures cargo into vesicles and mediates vesicle budding from the ER. Though Cargo recognition appears to be meditated primarily by the different isoforms of Sec24 (47), Sec23 and Sar1 also play a role in the recognition of a subset of cargos (48, 49). Here we found that Sec23B, Sar1A, and Sar1B were also upregulated upon OPC differentiation. It raises the question of whether specific upregulation of these COPII components will affect protein sorting or secretome of oligodendrocytes.

Autocrine PTN signaling functions downstream of Sec13 in OLs

By analysis of secretome of OPCs and differentiating immature oligodendrocytes, we showed that OL secreted more factors upon differentiation induction, whereas knockdown of Sec13 strongly inhibited these secretions. We further identified PTN as an autocrine factor to promote OL development. Instead of impacting PTN transcription level, loss of Sec13 impaired PTN secretion and caused PTN accumulation in ER. We also observed that PTN concentrated to the ERES upon differentiation. Through addition of recombinant PTN protein and ectopic PTN expression, we provide evidence that OLs are able to promote its own differentiation via autocrine PTN. Oligodendrocytes secrete a large amount of factors according to our identified secretome. The secretome also alters upon differentiation. It would be intriguing to characterize the functions of secreted factors under different developmental states. Compared to paracrine by factors released by neuron or astrocytes, autocrine regulation has the advantage of spatial proximity of signals. It is reported that hypoxia or HIF1α stabilization activates cell-autonomous Wnt production and inhibits OPC maturation (50). Our finding provides another example that OPCs regulate its own differentiation by autocrine signaling and also highlights the complexity of regulatory mechanisms of myelinogenesis.

Potential roles for PTN in remyelination

PTN is a developmentally regulated factor that have diverse roles in brain development (39). It has been shown to function through several transmembrane receptors, such

as PTPRZ, ALK, SDC3, and LRP1. By immunoprecipitation, we found that only PTPRZ interacts with endogenous PTN in differentiating immature oligodendrocytes. PTPRZ is an abundant phosphatase in OPCs and negatively regulate OPC maturation through its phosphatase activity (46). Furthermore, p190RhoGAP, which is a downstream dephosphorylating substrate of PTPRZ, can be quickly activated by PTN and induce OL process extension. In this study, we observed a dramatic upregulation of PTN in OL lineage upon LPC-induced demyelinating injury, indicating a potential role of PTN in remyelination. More importantly, ectopic expression of PTN by retrovirus accelerated remyelination rate in LPC-induced demyelinating mouse model. Further studies are needed to determine whether infusion of PTN or bioactive mimic is able to promote remyelination in other demyelinating models and human demyelinating diseases.

Methods

Mice. *Sec13*$^{flox/flox}$ mice were generated by crossing hypomorphic Sec13 mice with FLPe-expressing transgenic mice to remove NEO cassette (27). Mice homozygous for floxed alleles of *Sec13*$^{flox/flox}$ were crossed with Olig1-cre$^{+/-}$ mice to generate *Sec13*cKO (*Sec13* $^{flox/flox}$*; Olig1-Cre*$^{+/-}$) and heterozygous control (*Sec13* $^{flox/+}$; *Olig1-Cre*$^{+/-}$) mice (28). Heterozygous mice were used as control since they developed and behaved the same as WT. *NG2-CreERT* mice (51) or PDGFRα-CreERT (19) were crossed with *Sec13*$^{flox/flox}$ mice using similar mating strategy to generate the OPC-specific iKO mice. *Sec13*$^{flox/flox}$ mice receiving tamoxifen were used as control. All animal procedures used in this study were performed in accordance with the protocol approved by the

Institutional Animal Care and Use Committee at Xiamen University. Animals were housed in a 12-hour light/dark cycle with free access to water and food. All mice in the study were backcrossed to the C57BL/6 background for at least six generations.

Antibodies and reagents. The following antibodies were used: Goat anti-MBP (Cat#sc-13914; Santa cruz), Mouse anti-CC1 (Cat#op-80; Millipore), Rabbit anti-PDGFRα (Cat# sc-338; Santa cruz), Rabbit anti-GFAP (Cat# AP0123; Ascend), Mouse anti-mAb414 (Cat# 902901; Biolegend), Goat anti-Olig2 (Cat# AF2418; R&D systems), Mouse anti-NeuN (Cat# MAB377; Millipore), Rabbit anti-CNP (Cat#13427-1-AP; Proteintech), Rat anti-BrdU (Cat# ab6326; Abcam), Rat anti-Ki67 (Cat# 14-5698-82; Thermo), Rabbit anti-Sec13 (Cat# A303-980A; BETHYL LABORATORIES), Mouse anti-Sec13 (Cat# sc-7392; Santa cruz), Mouse anti-CNPase (Cat# C5922; Sigma), Rabbit anti-Olig2 (Cat#AP0337; Talent Biomedical), Rabbit anti-HA (Cat# 51064-2-AP; Proteintech), Rabbit anti-MBP (Cat#BA0094; BOSTER), Mouse anti- PTN (Cat# sc-74443; Santa Cruz), Rabbit anti-Flag (Cat#20543-1-AP; Proteintech), Rabbit anti-Sec23A (Cat# 8162; Cell Signaling Technology), Rabbit anti-Sec23B (Cat# ab151258; Abcam), Anti-Sec24A (Cat# 15958-1-AP; Proteintech), Rabbit anti-Sec24B (Cat# ab240703; Abcam), Rabbit anti-Sar1A (Cat# 15350-1-AP; Proteintech), Rabbit anti-Sar1B (Cat# 22292-1-AP; Proteintech), Rabbit anti-Nup107 (Cat# 19217-1-AP; Proteintech), Mouse anti-Tubulin (Cat# 66031-1-Ig; Proteintech), Mouse anti-Sec31A (Cat# 612351; BD Biosciences), Rabbit anti-Nup62 (Cat# 13916-1-AP; Proteintech), Mouse anti-GAPDH (Cat# 60004-1-Ig; Proteintech), Rabbit anti-Nup88 (Cat# 55465-

1-AP; Proteintech), Rabbit anti-Nup205 (Cat# 24439-1-AP; Proteintech), Mouse anti-β-Actin (Cat# CL594-66009; Proteintech), Mouse anti-Bip (Cat# 66574-1-Ig; Proteintech), Rabbit anti-p-eIF2a (Cat# ab32157; Abcam), Rabbit anti-eIF2a (Cat# 11233-1-AP; Proteintech), Rabbit anti-CHOP (Cat# 15204-1-AP; Proteintech), Mouse anti-Atf4 (Cat# CL594-60035; Proteintech), Rabbit anti-Atf6 (Cat# 24169-1-AP; Proteintech), Rabbit Anti-PDI (Cat#11245-1-AP; Proteintech), Rabbit anti-PTPRZ1 (Cat# 55125-1-AP; Proteintech), Rabbit anti-SDC3 (Cat# A18312; ABclonal), Rabbit anti-LRP1 (Cat# A0633; ABclonal), Rabbit anti-Integrin α V (Cat# A19071; ABclonal), Rabbit anti-ALK (Cat# A0766; ABclonal), Rabbit anti-p-p190 Y1105 (Cat# P30433; BOSTER), Rabbit anti-p190 (Cat# 26789-1-AP; Proteintech), Rabbit anti- p-PI3K (Cat# 4228; Cell Signaling Technology), Rabbit anti- PI3K (Cat# 3358; Cell Signaling Technology), Mouse anti-p-Stat3 Y705 (Cat# 4113; Cell Signaling Technology), Mouse anti-Stat3 (Cat# 9132; Cell Signaling Technology), Rabbit anti-p-GSK-3β(S9) (Cat# 9336; Cell Signaling Technology), Rabbit anti-GSK3β (Cat# 9332; Cell Signaling Technology), Rabbit anti-p-ERK1/2(T202/Y204) (Cat# 4376; Cell Signaling Technology), Rabbit anti-ERK1/2 (Cat# 9102; Cell Signaling Technology), Rabbit anti-p-β-Catenin(S45) (Cat# 9564; Cell Signaling Technology), Mouse anti-β-Catenin (Cat# c19220; Cell Signaling Technology), Rabbit anti-p-AKT(S473) (Cat# 9271; Cell Signaling Technology), Mouse anti-AKT (Cat# CL488-60203; Proteintech), Rabbit anti-p-Fyn(Y416) (Cat# 2102; Cell Signaling Technology), Mouse anti-ribosomal proteins s6 (Cat# sc-74576; Santa cruz), Rabbit anti-Phospho-S6 ribosomal protein (Cat# 2211; Cell Signaling Technology), Rabbit anti-FYN (Cat# CL488-66606; Proteintech), Cy2™

AffiniPure Donkey Anti-Mouse IgG (H+L) (Cat# 715-225-151; Jackson Immuno Research Laboratories), Cy3™ AffiniPure Donkey Anti-Rabbit IgG (H+L) (Cat# 711-165-152; Jackson Immuno Research Laboratories), Cy5™ AffiniPure Donkey Anti-Goat IgG (H+L) (Cat# 705-175-147; Jackson Immuno Research Laboratories). The following reagents were used: T3 RNA polymerase (Cat# P208C; Promega), DIG RNA label mix (Cat#11277073910; Roche), LPC (Cat# L4129; Sigma), Tamoxifen (Cat# T5648; Sigma), Prolong Gold Antifade Mountant (Cat# P36934; ThermoFisher), PTN (100 nM, Cat# 51000; Sinobiological), PDGF-AA (Cat# 100-13A; Peprotech), bFGF (Cat# 10014-HNAE; Sino Biological), NT3 (Cat# 450-03; Peprotech), LIF (50 ng/mL, Cat# 50756; Sinobiological), APOE (15 μg/mL, Cat# 10817-H30E; Sinobiological), MDK (100 nM, Cat# 10247; Sinobiological), CSAD (250 ng/mL, Cat#H00051380-Q01; NOVUS), Fluoromyelin (Cat#F34652; ThermoFisher), BFA (Cat#50502ES03; YEASON), CNTF (Cat# 450-13; Peprotech), TUNEL kit (Cat# A113-03; Vazyme).

Western blot. Protein from each sample was separated on 10%-15% SDS-PAGE gels and transferred onto PVDF membranes. Membranes were blocked with 5% non-fat milk powder in TBS containing 0.1% Tween 20 for 1 hour, followed by incubation with primary antibodies at 4°C overnight. After washing, membranes were incubated with HRP-conjugated secondary antibodies and developed using an ECL chemiluminescence detection system according to the instructions of the manufacturer.

Cell cultures and analyses. Primary mouse OPCs were isolated as described (52).

Briefly, P4-P7 mouse cortices cells were obtained by immunopanning with antibodies against GalC and O4 coated plates sequentially. Rat OPCs were isolated from cortices of pups at P2-P4 as mouse OPCs with slight modifications. Briefly, mixed cortices cells were obtained by immunopanning with antibodies against GalC and A2B5 coated plates sequentially. Isolated OPCs were grown in the OPC Growth Medium (OGM, DMEM/F-12 (GIBCO) with addition of 2% B-27 (GIBCO), 1% N2 (GIBCO), 20 ng/ml PDGF-AA (Peprotech, 100-13A), 10 ng/ml CNTF (Peprotech, 450-13), 20 ng/ml bFGF (Sino Biological, 10014-HNAE), 5 μM Forskolin (Sigma, F6886), 10 ng/ml Biotin (Sigma, B4639), 5 μg/ml Insulin (Sigma, I-6634), Trace Elements B (CORNING, 16615008), Sodium Pyruvate (Invitrogen, 11360-070), Penicillin-streptomycin (Invitrogen, 15140-122) and 1 ng/ml NT3 (Peprotech, 450-03)). OPCs was differentiated using OPC Differentiation Medium (ODM). This medium differed from the OGM: Triiodothyronine (T3) (60 nM) was added and PDGF-AA, bFGF and NT3 were removed.

Primary microglial cultures were obtained by microdissection from brains of <2-day-old neonatal mice. Brains were mechanically minced and dissociated with 0.25% trypsin. The tissue suspension was passed through a 70 μm nylon cell strainer. Cell pellets were harvested and resuspended in DMEM supplemented with 10% heat-inactivated FBS and plated on poly-L-lysine pre-coated culture flasks. After 3 days, medium was changed, containing 25 ng/mL GM-CSF and 10% FBS. Primary microglial cells were harvested by shaking (200 rpm, 20 min) after 10-12d in culture, and every 3 days thereafter. Primary astrocytes were cultured in astroglial medium

(Dulbecco's modified eagle medium/Nutrient mixture F-12 (DMEM/F12) (1:1) (GIBCO) with 10% FBS. Contaminating cells in the astroglia monolayer were removed by overnight shaking at 220 rpm at 37°C.

Oli-neu cells (53) were cultured in Oli-neu medium, which contained DMEM/F-12 supplemented with 2% B-27, 1% N2, 5% FBS (GIBCO), 1% horse serum (GIBCO), 7.2 mM Glucose and 1× penicillin-streptomycin. The 293T (from the American Type Culture Collection) were maintained in DMEM supplemented with 10% FBS and 1× penicillin-streptomycin. Sinofection (Sino Biological, STF02) was used as transfection reagent for 293T. The electroporation was performed in a cuvette provided in the Nucleofector Kit using a Lonza Nucleofector 2b device (LONZA, O-017) according to the manufacturer's protocol. Approximately 2.0 × $10^{\wedge 6}$ OPCs or Oli-neu in 100 μL Basic Nucleofector™ Kit for Primary Mammalian Glial Cells (Lonza, VPI-1006) were resuspended. 5 μg of plasmids or 5 μl of 20 μM siRNA was used for each transfection. Generally, cells were kept in growth medium for 24 hours after electroporation and then incubated in differentiating medium for 48 or 72 hours.

RNA extraction and qRT-PCR. Total RNA was extracted according to the Trizol (Life Technologies) protocol and cDNA were produced with 5X All-In-One RT MasterMix (ABM). Primer sequences used for identifying (I) the allele containing NEO cassette: *Neo-f*, ATGTGTCAGTTTCATAGCCTGAAG, *Neo-r*, CAGGTGAGGGTTCCAAGACC; (II) the allele deleted of NEO cassette: *dNeo-f*, GCTAATAAAATCATATTGCA, *dNeo-r*, CAGGTGAGGGTTCCAAGACC. Real-time PCR was carried out using the Bio-Rad

579 Real-Time PCR System with ChamQ Universal SYBR qPCR Master Mix (Vazyme).
580 Primer sequences used for rat gene were: *Gapdh-f*, TCCAGTATGACTCTACCCACG,
581 *Gapdh-r*, CACGACATACTCAGCACCAG; *Cnp-f*, CTACTTTGGCAAGAGACCTCC,
582 *Cnp-r*, AGAGATGGACAGTTTGAAGGC; *Plp-f*, TCTTTGGCGACTACAAGACCACCA,
583 *Plp-r*, CAAACAATGACACACCCGCTCCAA; *Mbp-f*,
584 TTGACTCCATCGGGCGCTTCTTTA, *Mbp-r*, TTCATCTTGGGTCCTCTGCGACTT;
585 *Sec13-f*, GGTCACCTAAACTCCTACACAAG, *Sec13-r*,
586 CATCCACCGACTCTTTCCAC; *Sec23A-f*, GAGCAAAACTCTGGGCTTGC, *Sec23A-r*,
587 GGGACCACGCAGAACTACAT; *Sec23B-f*, AGAACGAGATGGTGTGCGTT, *Sec23B-r*,
588 GGTAAGTCTGGGCGCTCTTT; *Sec24A-f*, TCCCCGAATGGCACTACCTA, *Sec24A-r*,
589 GTCTGTGGTCCTGTGGATGG *Sec24B-f*, CAGCAATTAACGAAAATGTCCAAC,
590 *Sec24B-r*, TGCCTTTTGTCTGCATCTGCT; *Sar1A-f*, GGCTCTATGGGCAAACCACA,
591 *Sar1A-r*, CCTTGCCTCTTGAGCACACT; *Sar1B-f*, CGTCCCAACACTACATCCCA,
592 *Sar1B-r*, TCCATACTCTTCGGGCTTGC; *Sec31A-f*, CAGCCAGCCACCACCTTATC,
593 *Sec31A-r*, AGAAGCAGGAGGAGCAACAG; *Sec31B-f*,
594 TCACGGCCAAGTGAGAAGAC, *Sec31B-r*, TCTTCAGGCATGTGTCCACC; *PTN-f*,
595 GGCTTGGGGAGAATGTGACC, *PTN-r*, ACAGGGCTTGGAGATGGTGA; *P190-f*,
596 TAGCATCCGAAAGAGCCGGT, *P190-r*, GCCATCAGTGAGTGCGACAA; for mouse
597 gene sequences were: *Gapdh-f*, TGCCAAATATGATGACATCAAGAA, *Gapdh-r*,
598 GGAGTGGGTGTCGCTGTTG; *Sec13*-f, GACTGGGTCCGAGATGTTG, *Sec13*-r,
599 ACTTGTGTAGGAGTTTAGGTGAC; *Mbp-f*, TCACAGAAGAGACCCTCACA; *Mbp-r*,
600 GCCGTAGTGGGTAGTTCTTG; *Cnp1-f*, TCCACGAGTGCAAGACGCTATTCA, *Cnp1-*

r, TGTAAGCATCAGCGGACACCATCT; *Plp-f*, TGCTCGGCTGTACCTGTGTACATT, *Plp-r*, TACATTCTGGCATCAGCGCAGAGA; *Mog-f*, AGATGGCCTGTTTGTGGAG, *Mog-r*, TTCATCCCCAACTAAAGCCC; *Myrf-f*, CAGACCCAGGTGCTACAC, *Myrf-r*, TCCTGCTTGATCATTCCGTTC.

Tissue and immunohistochemistry. Mice were anesthetized before sacrifice. The brain and spinal cord were dissected, fixed with 2% paraformaldehyde (PFA) for 6-8 hours and dehydrated in 30% sucrose. Tissues were embedded in O.C.T. compound (CellPath) and sliced into 12-μm sections using cryostat. Cryosections were permeabilized and incubated with blocking solution (0.4% Triton X-100 and 3% normal BSA in PBS) for 1 hour at room temperature (RT) and overlaid with primary antibodies with various dilution ratio overnight at 4°C. Sections were incubated with secondary antibodies, which conjugated to Cy2, Cy3 and Cy5 before mounting. Immunofluorescence images were obtained with confocal laser microscope (Leica SP8, Zeiss LSM 880 Airy scan or Zeiss LSM 780). For immunostaining of cells, cells were first fixed by 2% PFA for 30 mins at RT. Subsequently, cells were permeabilized with the 0.5% Triton X-100 in PBS at 4°C, then blocked by 3% BSA in PBS. The samples were incubated with primary antibodies overnight at 4°C. After wash in PBS, secondary antibodies were used for RT 1 hour before mounting with ProLong Gold Antifade Reagent (Invitrogen). For in situ hybridization, cryosections were incubated with the digoxigenin (DIG)-labeled RNA antisense probe for murine *Plp1/Dm-20* as described previously (54). The probes were prepared with DIG RNA labelling Kit

623 (Roche, 11277073910). An anti-DIG antibody conjugated with alkaline phosphatase
624 (Roche, 11093274910) was used to probe sections. Nitro blue tetrazolium (NBT) and
625 5-bromo-4-cloro-3-indolyl phosphate (BCIP) (Sangon, A600116) were used as
626 substrates to develop.

627 *Oligo d(T) in situ hybridization* was performed as described (32). Briefly, cells
628 were fixed with paraformaldehyde and permeabilized with Triton X-100. Then the
629 hybridization was performed at 42°C overnight with a cy3-labeled oligo (dT) probe.
630 Samples were washed with 2 × and 0.5× SSC at 42°C, then stained with DAPI and
631 mounted on glass slides.

632

633 *Lysolecithin-induced demyelinating injury.* Lysolecithin (LPC)-induced
634 demyelination was carried out in the corpus callosum or spinal cord of 10-week-old
635 mice as described previously (31). Briefly, 1 μl 1% LPC was injected into the
636 ventrolateral white matter in spinal cord between the Th3-Th4 with a Hamilton syringe.
637 For demyelination in the brain, demyelinating lesions were induced by micro-injection
638 1.5 μl 1% LPC into corpus callosum at the following coordinates: 1.0 mm backward to
639 bregma, 1.0 mm lateral to bregma, and 1.5 mm deep relative to skull surface. Titers of
640 lentivirus and retrovirus were estimated to be ~$1.0X10^5$/μl and 1 μl virus was injected
641 by mixing with LPC in indicated experiments. Mice were sacrificed at different time
642 points after injury. For TUDCA treatment in LPC injury assay, mice were treated with
643 TUDCA (500 mg kg^{-1}) by gavage over 11 consecutive days. Ethidium bromide (EB)-
644 induced demyelination was similarly carried out as LPC injury assay. 1.5 μl 1% EB was

645 micro-injected into the same regions as LPC assay.

646

647 *Tamoxifen administration.* Tamoxifen (20 mg/mL) was prepared in corn oil and
648 stored at -20°C. A dose of 40 μg/g (grams, body weight) was i.p. injected into newborn
649 mice once a day from p3 to p5 for 3 days. For LPC assay, 8-10 weeks mice were
650 treated with tamoxifen (200 μg/g) by gavage over 7 consecutive days.

651

652 *Plasmids and viruses preparation.* Mouse *Sec13* (gene ID: 110379), rat *Sec13*
653 (gene ID: 297522), rat *Sec31A* (gene ID: 93646), mouse *PTN* (gene ID: 19242), rat
654 *PTN* (gene ID: 24924) were cloned into the vector either pcDNA3.3, RV-GFP or pCDH-
655 MSCV-T2A-copGFP vectors. The PTN-L18/20R construct was established by
656 mutating amino acid leucine (L) at 18^{th} and 20^{th} to arginine (R). Lentiviruses were
657 generated by transfecting 293T cells with the lentiviral vector pLKO.1 and packaging
658 plasmids. Retroviruses were generated by transfecting 293T cells with the retroviral
659 vector and packaging plasmids. Viruses were concentrated by ultracentrifuge.

660

661 *Immunoprecipitation.* Cells were washed twice with ice cold PBS
662 and were scrapped off with PBS supplemented with protease inhibitors 1 mM PMSF.
663 For each sample, approximately 1.0 x 10^7 cells were lysed with 1 ml Co-IP buffer
664 (50 mM Tris-HCl pH 7.5, 150 mM NaCl, 1 % Triton X-100, 1 mM EDTA, 0.0 1 mM NaF,
665 0.01 mM Na_3VO_4) with 1 mM PMSF for 1h. Samples were then briefly sheared by
666 sonication for 10 times (1 s on, 1 s off, power=25%). After centrifugation at 4°C for 15

min at 14,000 x g, 5% supernatants were boiled with 4x SDS as input and the left was incubated with 2μg antibody overnight. Immunoprecipitated complexes were collected using 30 μl 50% slurry proteinA/G plus agarose beads (Millipore) at 4°C for 2h. Beads were washed three times with Co-IP buffer. After washing, beads were resuspended in 30 μl 2x SDS and boiled in 95°C for 15 min for elution.

Conditioned medium. 80% confluent microglia, astrocytes and rat iOLs (differentiated 48 hours) were washed three times with PBS and changed to DMEM/F-12 for 24 hours to collect secreted proteins. Collected DMEM/F-12 medium was centrifuged at 2000 rpm for 5 min and filtered with 0.45 μm filters to removed cell debris. Each 20 mL DMEM/F-12 from these glia cells and 20 mL fresh DMEM/F-12 were concentrated to 1.8 mL with Amicon® Ultra-15 Centrifugal Filter (MERCK). For PTN depletion, concentrated medium was incubated with 2μg PTN antibody overnight following incubation with 30 μl 50% slurry protein A/G plus agarose beads (Millipore). The sample was centrifuged to remove PTN. 0.2 mL 10×OPC Differentiation Medium components (without T3) in DMEM/F-12 was added to concentrated medium to make conditioned medium. 1×10^6 rat OPCs in 35mm dish were treated with conditioned medium for 48 hours.

Electron microscopy. Tissue or cell processing was performed essentially as described previously (31). Briefly, mice were anesthetized and perfused with pre-cold sodium cacodylate buffer. Optic nerves, corpus callosum and spinal cord were

689 immediately dissected and immersed in a pre-cooled fixation buffer (2.5%
690 glutaraldehyde, 0.1 M phosphate buffer (PB), pH 7.4) overnight at 4°C. As for OPCs,
691 cells were directly dissociated and collected as sedimentary bulks, which were then
692 fixed as above. After being washed in PB, samples were successively treated with
693 OsO_4 (1% OsO_4 in PB), serially dehydrated in ethanol, and finally embedded in Spurr's
694 resin to obtain the blocks. The blocks were then sectioned into 70-nm slices and
695 stained with lead citrate for electron microscopy imaging by using Hitachi HT-7800
696 (Hitachi, Minato-ku, Tokyo, JAPAN).
697
698 *LS-MS/MS of conditioned medium.* Each group contained three duplications. For
699 each sample, rat OPCs ($3X10^{\wedge 6}$ cells) were differentiated with ODM for 48 hours, then
700 washed three times with PBS and changed to DMEM/F-12 for 3 hours to collect
701 secreted proteins. The supernatants were mixed with 20% volume of 100% w/v
702 trichloroacetic acid (TCA) and incubated at 4°C overnight. The protein pellet was
703 collected by centrifugation at 15000 rpm for 15 min and washed with pre-cooled
704 acetone, finally followed by centrifugation at 15000 rpm for 10 min. The wash step was
705 repeated twice. Then the protein pellet was diluted with 1% Sodium Deoxycholate in
706 0.1 M Tris pH8.0 and the concentrations were determined using the BCA Protein
707 Quantification Kit (Vazyme). Label-free protein quantification was performed using
708 TripleTOF 5600 LS-MS/MS system (AB Sciex).
709
710 *Statistics.* Data are presented as arithmetic mean ± SEM. Statistical analyses

were performed with GraphPad Prism 6 and significance was set at $P < 0.05$ using two-tailed unpaired Student's *t* tests or 1-way ANOVA with Tukey's correction for multiple comparisons (See each figure for details). Each experiment was done by analyzing at least three different experimental groups in a blinded fashion.

Study approval. The care and treatment of animals were approved by the Institutional Animal Care and Use Committee at Xiamen University.

Author contributions

LZ, ZW and WM conceived and designed the study and experiments. ZL, MY, WL, RJ, WD, JC, CW, LL, MW, XL, CW, CX, LY, CW, JH, and NX performed the experiments. ZL, MY, and LZ analyzed data. LZ wrote the manuscript. LZ supervised the study. The order of co-first authors was determined by the volume of work each contributed to the study.

Acknowledgments

We thank Qingfeng Liu, Lixin Hong, Wei Han and Chuanqi Zhong for technical support, William D. Richardson and Huiliang Li (University College London) for experimental resource. This study was funded by grants from the National Natural Science Foundation of China 31872642，32170966 to L.Z., the Fundamental Research Funds for the Central Universities 20720190072 to L.Z., the National Key R&D Program of China (2021YFA1101401 to W.M.).

Competing interests

The authors have declared that no conflict of interest exists.

Address correspondence to: Zhanxiang Wang, Department of Neurosurgery, Xiamen Key Laboratory of Brain Center, The First Affiliated Hospital of Xiamen University, The Department of Neuroscience, Institute of Neurosurgery, School of Medicine, Xiamen University, Xiamen, Fujian 361003, P.R. China. Phone: 86-0592-2137275 Email: wangzx@xmu.edu.cn Or to: Liang Zhang, State Key Laboratory of Cellular Stress Biology, The First Affiliated Hospital of Xiamen University, Innovation Center for Cell Signaling Network, School of Life Sciences, Xiamen University, Xiamen, Fujian 361102, China. Phone: 86-18259240741 Email: lzhangxmu@xmu.edu.cn

References

1. Bradl M, and Lassmann H. Oligodendrocytes: biology and pathology. *Acta Neuropathol.* 2010;119(1):37-53.
2. Bercury KK, and Macklin WB. Dynamics and mechanisms of CNS myelination. *Dev Cell.* 2015;32(4):447-58.
3. Trapp BD, and Nave KA. Multiple sclerosis: an immune or neurodegenerative disorder? *Annu Rev Neurosci.* 2008;31:247-69.
4. Chang A, et al. Premyelinating oligodendrocytes in chronic lesions of multiple sclerosis. *N Engl J Med.* 2002;346(3):165-73.
5. Venditti R, et al. Exiting the ER: what we know and what we don't. *Trends Cell Biol.* 2014;24(1):9-18.
6. Zanetti G, et al. COPII and the regulation of protein sorting in mammals. *Nat Cell Biol.* 2011;14(1):20-8.
7. Korpal M, et al. Direct targeting of Sec23a by miR-200s influences cancer cell secretome and promotes metastatic colonization. *Nat Med.* 2011;17(9):1101-8.
8. Saito A, et al. Regulation of endoplasmic reticulum stress response by a BBF2H7-mediated Sec23a pathway is essential for chondrogenesis. *Nat Cell Biol.* 2009;11(10):1197-204.
9. Chen XW, et al. SEC24A deficiency lowers plasma cholesterol through reduced PCSK9 secretion. *Elife.* 2013;2:e00444.
10. Lang MR, et al. Secretory COPII coat component Sec23a is essential for craniofacial chondrocyte maturation. *Nat Genet.* 2006;38(10):1198-203.
11. Merte J, et al. Sec24b selectively sorts Vangl2 to regulate planar cell polarity during neural tube closure. *Nat Cell Biol.* 2010;12(1):41-6; sup pp 1-8.
12. Wang B, et al. The COPII cargo adapter SEC24C is essential for neuronal homeostasis. *J Clin Invest.* 2018;128(8):3319-32.
13. Yang XY, et al. Mutations in the COPII vesicle component gene SEC24B are associated with human neural tube defects. *Hum Mutat.* 2013;34(8):1094-101.

14. Halperin D, et al. SEC31A mutation affects ER homeostasis, causing a neurological syndrome. *J Med Genet.* 2019;56(3):139-48.
15. Baron W, and Hoekstra D. On the biogenesis of myelin membranes: sorting, trafficking and cell polarity. *FEBS Lett.* 2010;584(9):1760-70.
16. Emery B. Regulation of oligodendrocyte differentiation and myelination. *Science.* 2010;330(6005):779-82.
17. Pringle N, et al. PDGF A chain homodimers drive proliferation of bipotential (O-2A) glial progenitor cells in the developing rat optic nerve. *EMBO J.* 1989;8(4):1049-56.
18. Barres BA, and Raff MC. Control of oligodendrocyte number in the developing rat optic nerve. *Neuron.* 1994;12(5):935-42.
19. Rivers LE, et al. PDGFRA/NG2 glia generate myelinating oligodendrocytes and piriform projection neurons in adult mice. *Nat Neurosci.* 2008;11(12):1392-401.
20. Richardson WD, et al. NG2-glia as multipotent neural stem cells: fact or fantasy? *Neuron.* 2011;70(4):661-73.
21. Fancy SP, et al. Dysregulation of the Wnt pathway inhibits timely myelination and remyelination in the mammalian CNS. *Genes Dev.* 2009;23(13):1571-85.
22. Uppala JK, et al. Chemical chaperone, TUDCA unlike PBA, mitigates protein aggregation efficiently and resists ER and non-ER stress induced HepG2 cell death. *Sci Rep.* 2017;7(1):3831.
23. Perlmutter DH. Chemical chaperones: a pharmacological strategy for disorders of protein folding and trafficking. *Pediatr Res.* 2002;52(6):832-6.
24. Pryer NK, et al. Cytosolic Sec13p complex is required for vesicle formation from the endoplasmic reticulum in vitro. *J Cell Biol.* 1993;120(4):865-75.
25. Townley AK, Schmidt K, Hodgson L, and Stephens DJ. Epithelial organization and cyst lumen expansion require efficient Sec13-Sec31-driven secretion. *J Cell Sci.* 2012;125(Pt 3):673-84.
26. Hughes H, et al. Organisation of human ER-exit sites: requirements for the localisation of Sec16 to transitional ER. *J Cell Sci.* 2009;122(Pt 16):2924-34.
27. Moreira TG, et al. Sec13 Regulates Expression of Specific Immune Factors Involved in Inflammation In Vivo. *Sci Rep.* 2015;5:17655.
28. Lu QR, et al. Common developmental requirement for Olig function indicates a motor neuron/oligodendrocyte connection. *Cell.* 2002;109(1):75-86.
29. Kang SH, et al. NG2+ CNS glial progenitors remain committed to the oligodendrocyte lineage in postnatal life and following neurodegeneration. *Neuron.* 2010;68(4):668-81.
30. Siniossoglou S, et al. A novel complex of nucleoporins, which includes Sec13p and a Sec13p homolog, is essential for normal nuclear pores. *Cell.* 1996;84(2):265-75.
31. Liu Z, et al. Nucleoporin Seh1 Interacts with Olig2/Brd7 to Promote Oligodendrocyte Differentiation and Myelination. *Neuron.* 2019;102(3):587-601 e7.
32. Zhang L, et al. Inhibition of pyrimidine synthesis reverses viral virulence factor-mediated block of mRNA nuclear export. *J Cell Biol.* 2012;196(3):315-26.
33. Bar-Peled L, et al. A Tumor suppressor complex with GAP activity for the Rag GTPases that signal amino acid sufficiency to mTORC1. *Science.* 2013;340(6136):1100-6.
34. Niu X, et al. Sec13 safeguards the integrity of the endoplasmic reticulum and organogenesis of the digestive system in zebrafish. *Dev Biol.* 2012;367(2):197-207.
35. Boyadjiev SA, et al. Cranio-lenticulo-sutural dysplasia is caused by a SEC23A mutation leading to abnormal endoplasmic-reticulum-to-Golgi trafficking. *Nat Genet.* 2006;38(10):1192-7.

36. Townley AK, et al. Efficient coupling of Sec23-Sec24 to Sec13-Sec31 drives COPII-dependent collagen secretion and is essential for normal craniofacial development. *J Cell Sci.* 2008;121(Pt 18):3025-34.
37. Merksamer PI, and Papa FR. The UPR and cell fate at a glance. *J Cell Sci.* 2010;123(Pt 7):1003-6.
38. Hetz C, and Papa FR. The Unfolded Protein Response and Cell Fate Control. *Mol Cell.* 2018;69(2):169-81.
39. Gonzalez-Castillo C, et al Pleiotrophin as a central nervous system neuromodulator, evidences from the hippocampus. *Front Cell Neurosci.* 2014;8:443.
40. Deuel TF, et al. Pleiotrophin: a cytokine with diverse functions and a novel signaling pathway. *Arch Biochem Biophys.* 2002;397(2):162-71.
41. Meng K, et al. Pleiotrophin signals increased tyrosine phosphorylation of beta beta-catenin through inactivation of the intrinsic catalytic activity of the receptor-type protein tyrosine phosphatase beta/zeta. *Proc Natl Acad Sci U S A.* 2000;97(6):2603-8.
42. Tanga N, et al. The PTN-PTPRZ signal activates the AFAP1L2-dependent PI3K-AKT pathway for oligodendrocyte differentiation: Targeted inactivation of PTPRZ activity in mice. *Glia.* 2019;67(5):967-84.
43. Kuboyama K, et al. Role of Chondroitin Sulfate (CS) Modification in the Regulation of Protein-tyrosine Phosphatase Receptor Type Z (PTPRZ) Activity: PLEIOTROPHIN-PTPRZ-A SIGNALING IS INVOLVED IN OLIGODENDROCYTE DIFFERENTIATION. *J Biol Chem.* 2016;291(35):18117-28.
44. Wolf RM, et al. Tyrosine phosphorylation of p190 RhoGAP by Fyn regulates oligodendrocyte differentiation. *J Neurobiol.* 2001;49(1):62-78.
45. Liang X, et al. Signaling from integrins to Fyn to Rho family GTPases regulates morphologic differentiation of oligodendrocytes. *J Neurosci.* 2004;24(32):7140-9.
46. Kuboyama K, et al. Inactivation of Protein Tyrosine Phosphatase Receptor Type Z by Pleiotrophin Promotes Remyelination through Activation of Differentiation of Oligodendrocyte Precursor Cells. *J Neurosci.* 2015;35(35):12162-71.
47. Miller E, et al. Cargo selection into COPII vesicles is driven by the Sec24p subunit. *EMBO J.* 2002;21(22):6105-13.
48. Aridor M, et al. Cargo selection by the COPII budding machinery during export from the ER. *J Cell Biol.* 1998;141(1):61-70.
49. Mancias JD, and Goldberg J. The transport signal on Sec22 for packaging into COPII-coated vesicles is a conformational epitope. *Mol Cell.* 2007;26(3):403-14.
50. Yuen TJ, et al. Oligodendrocyte-encoded HIF function couples postnatal myelination and white matter angiogenesis. *Cell.*158(2):383-96.
51. Zhu X, et al. NG2 cells generate both oligodendrocytes and gray matter astrocytes. *Development.* 2008;135(1):145-57.
52. Dugas JC, et al. Functional genomic analysis of oligodendrocyte differentiation. *J Neurosci.* 2006;26(43):10967-83.
53. Pereira GB, et al. Expression of myelin genes: comparative analysis of Oli-neu and N20.1 oligodendroglial cell lines. *J Neurosci Res.* 2011;89(7):1070-8.
54. Ma Q, et al. Mash1 and neurogenin1 expression patterns define complementary domains of neuroepithelium in the developing CNS and are correlated with regions expressing notch ligands. *The Journal of neuroscience : the official journal of the Society for Neuroscience.*

1997;17(10):3644-52.

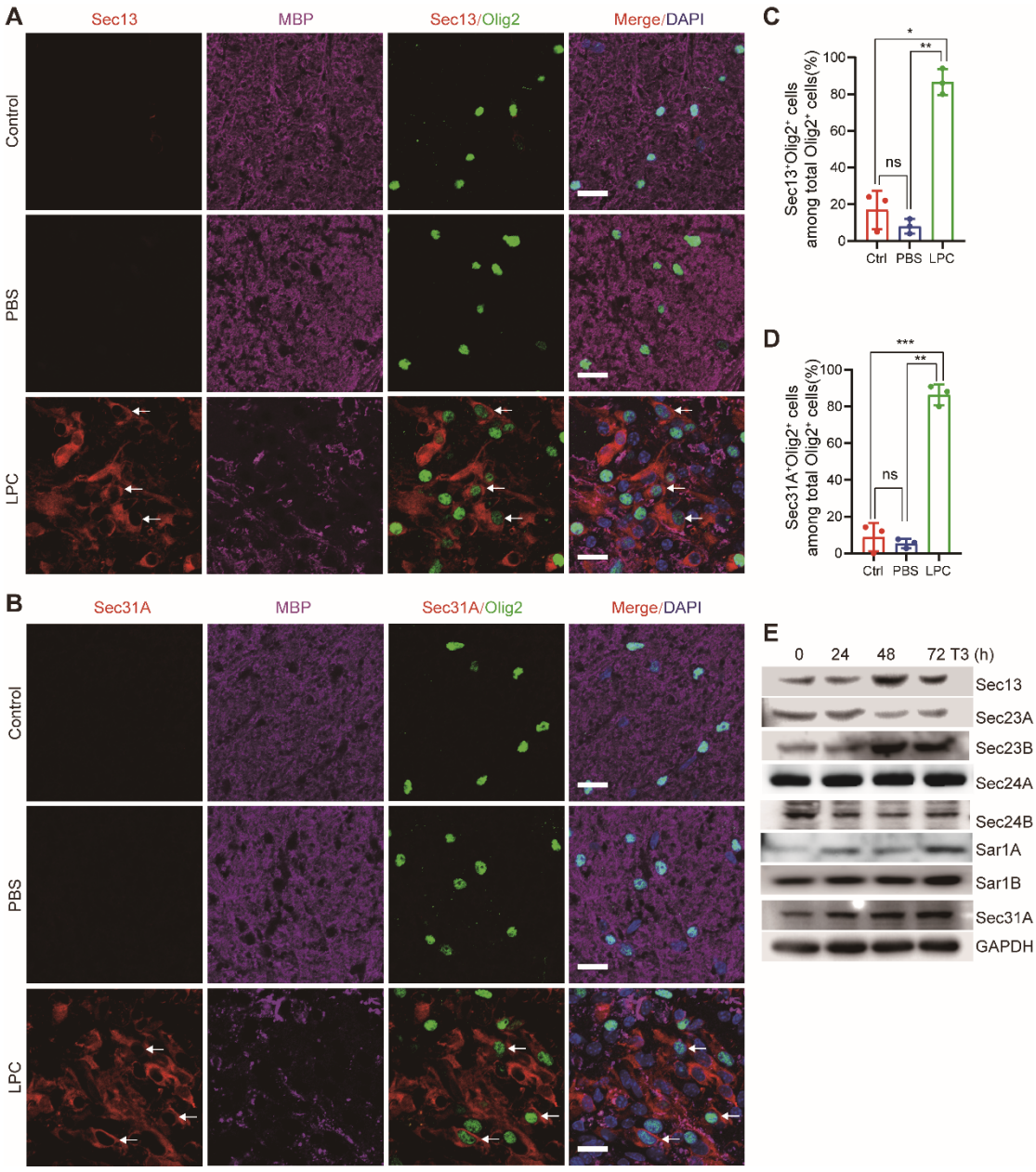

Figure 1. COPII complex is implicated in remyelination after demyelination.

(A) Immunostaining of Sec13, Olig2 and MBP at 7 dpl in non-lesion white matter control, PBS injection, and LPC lesion spinal cords from 8-week-old mice. Arrows indicate $Sec13^+/Olig2^+$ cells. Scale bars represent 20 μm.

(B) Immunostaining of Sec31A, Olig2 and MBP at 7 dpl in non-lesion white matter control, PBS injection, and LPC lesion spinal cords from 8-week-old mice. Arrows indicate $Sec31A^+/Olig2^+$ cells. Scale bars represent 20 μm.

(C-D) Quantification of $Sec13A^+$ $Olig2^+/Olig2^+$ cells (C) and $Sec31A^+$ $Olig2^+/Olig2^+$ cells (D) in LPC lesion sites (n= 3 animals/treatment). Ctrl=control. Data are represented mean ± SD and were analyzed by 1-way ANOVA with Tukey's correction for multiple comparisons.; *P<0.05, **P<0.01, ***P<0.001.

(E) Immunoblotting of indicated proteins in cultured rat OPCs and differentiating oligodendrocytes after T3 treatment.

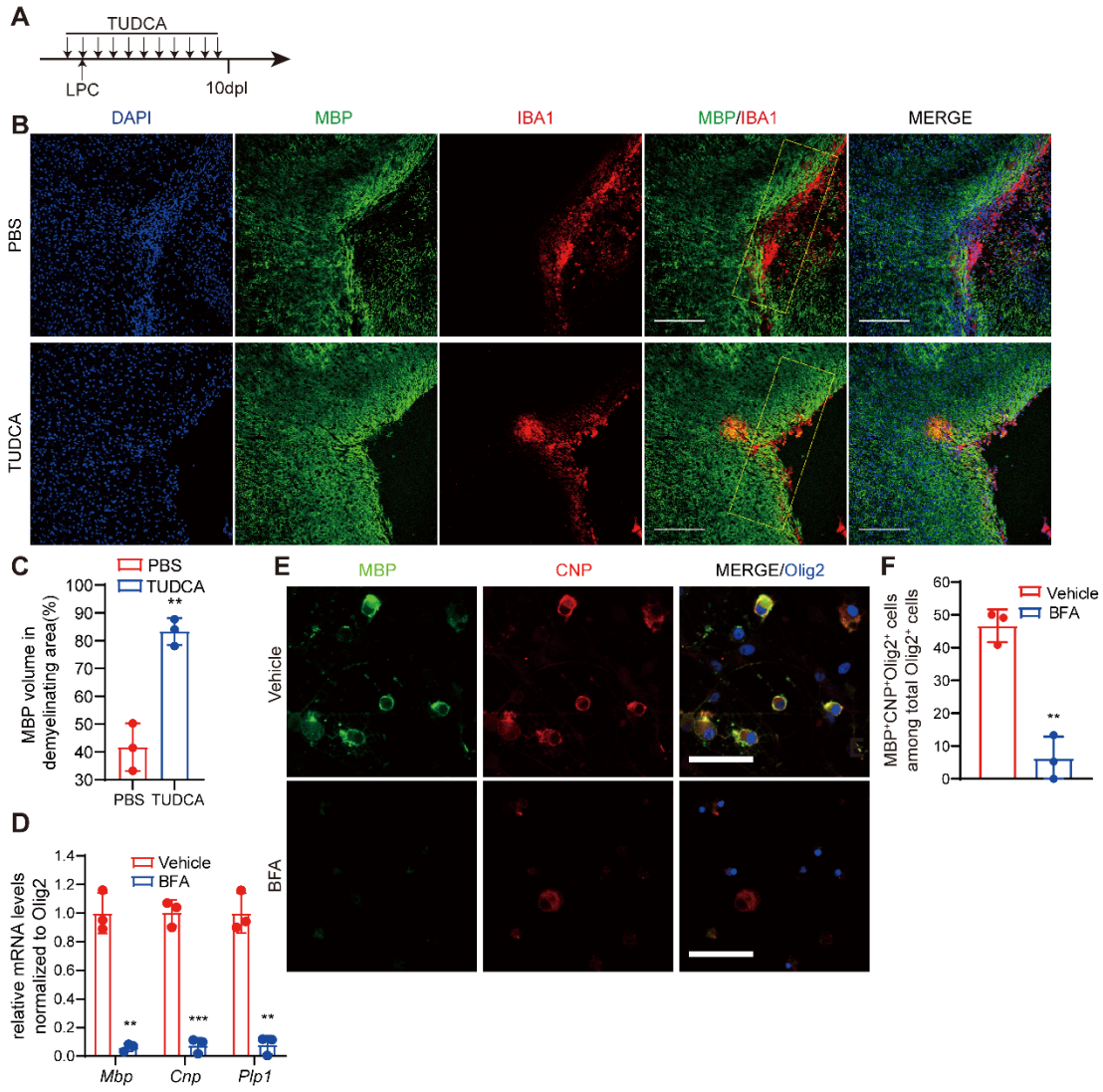

Figure 2. Protein transport is necessary for myelination.

(A) Diagram showing TUDCA administration and LPC injection schedule.

(B) Immunostaining of MBP and IBA1 in corpus callosum lesions of control and TUDCA-treated mice at 10 dpl. Scale bars represent 200 μm.

(C) Quantification of MBP$^+$ area in the demyelinating regions in corpus callosum of control and TUDCA-treated mice at 10 dpl (n= 3 animals/treatment).

(D) Real-time PCR analysis of myelination-associated genes in primary rat OPCs under differentiation conditions in the presence or absence of BFA (0.5 μg/μL). BFA was applied to cells when switching to differentiation media and incubated for 48 hours (n=3 independent experiments).

(E) Co-immunostaining of MBP, CNP and Olig2 in primary rat OPCs under differentiation conditions for 72 hours in the presence or absence of BFA (0.5 μg/μL). Scale bars represent 50 μm.

(F) Quantification of MBP$^+$ CNP$^+$ Olig2$^+$ cells as a percentage of total Olig2$^+$ cells after 3 d of differentiation (n= 3 independent experiments). Data are represented mean ± SD; $^{**}P$<0.01, $^{***}P$<0.001, two-tailed unpaired Student's t test.

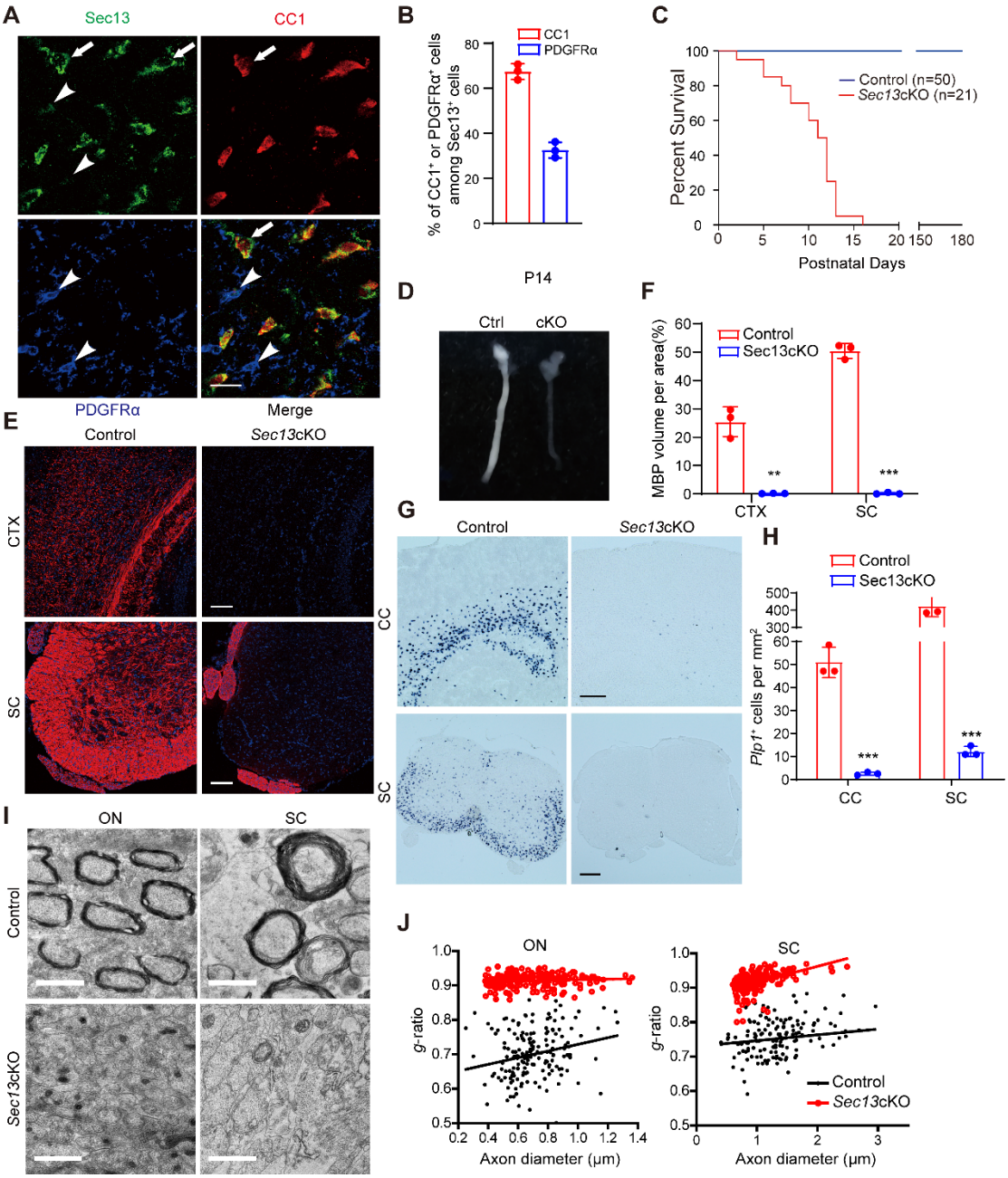
A
Sec13
CC1
B
CC1
PDGFRα
% of CC1+ or PDGFRα+ cells among Sec13+ cells
C
Control (n=50)
Sec13cKO (n=21)
Percent Survival
Postnatal Days
P14
D
Ctrl
cKO
F
Control
Sec13cKO
MBP volume per area(%)
CTX
SC
E
PDGFRα
Merge
Control
Sec13cKO
CTX
SC
G
Control
Sec13cKO
CC
SC
H
Control
Sec13cKO
Plp1+ cells per mm2
CC
SC
I
ON
SC
Control
Sec13cKO
J
ON
SC
g-ratio
Axon diameter (μm)
Control
Sec13cKO

Figure 3. COPII component Sec13 is required for myelination in the CNS.

(A) Co-immunostaining of Sec13, PDGFRα, and CC1 in the corpus callosum of wild-type mice at P14. Arrow indicates $Sec13^+$/ $CC1^+$ cells; arrowheads indicate $Sec13^+$/ $PDGFR\alpha^+$ cells. Scale bars represent 20 μm.

(B) Quantification of $CC1^+$ or $PDGFR\alpha^+$ cells among $Sec13^+$ cells in the corpus callosum at P14 (n= 3 wild type mice).

(C) Survival curves of control and *Sec13*cKO mice (n=50 control and 21 mutant mice).

(D) Representative images of optic nerves from control and *Sec13*cKO mice at P12.

(E) Immunostaining of MBP in the cortex (CTX), spinal cord (SC) of control and *Sec13*cKO at P14. Nuclei are stained with DAPI. Scale bars represent 100 μm.

(F) Quantification of MBP^+ volume in the cortex (CTX) or spinal cord (SC) of control and *Sec13*cKO mice at P14 (n= 3 control and 3 mutant animals).

(G-H) *In situ* hybridization (K) and quantification (L) of *Plp1* in the corpus callosum (CC) and spinal cord (SC) of control and *Sec13*cKO at P14 (n= 3 control and 3 mutant animals). Scale bars represent 250 μm.

(I) Electron micrograph analysis of optic nerves (ON) and spinal cord (SC) of control and *Sec13*cKO at P14. Scale bars represent 1 μm.

(J) The myelin *g*-ratio in optic nerves (ON) and spinal cord (SC) of control and *Sec13*cKO at P14. Data are represented mean ± SD; $^{**}P<0.01$, $^{***}P<0.001$, two-tailed unpaired Student's t test.

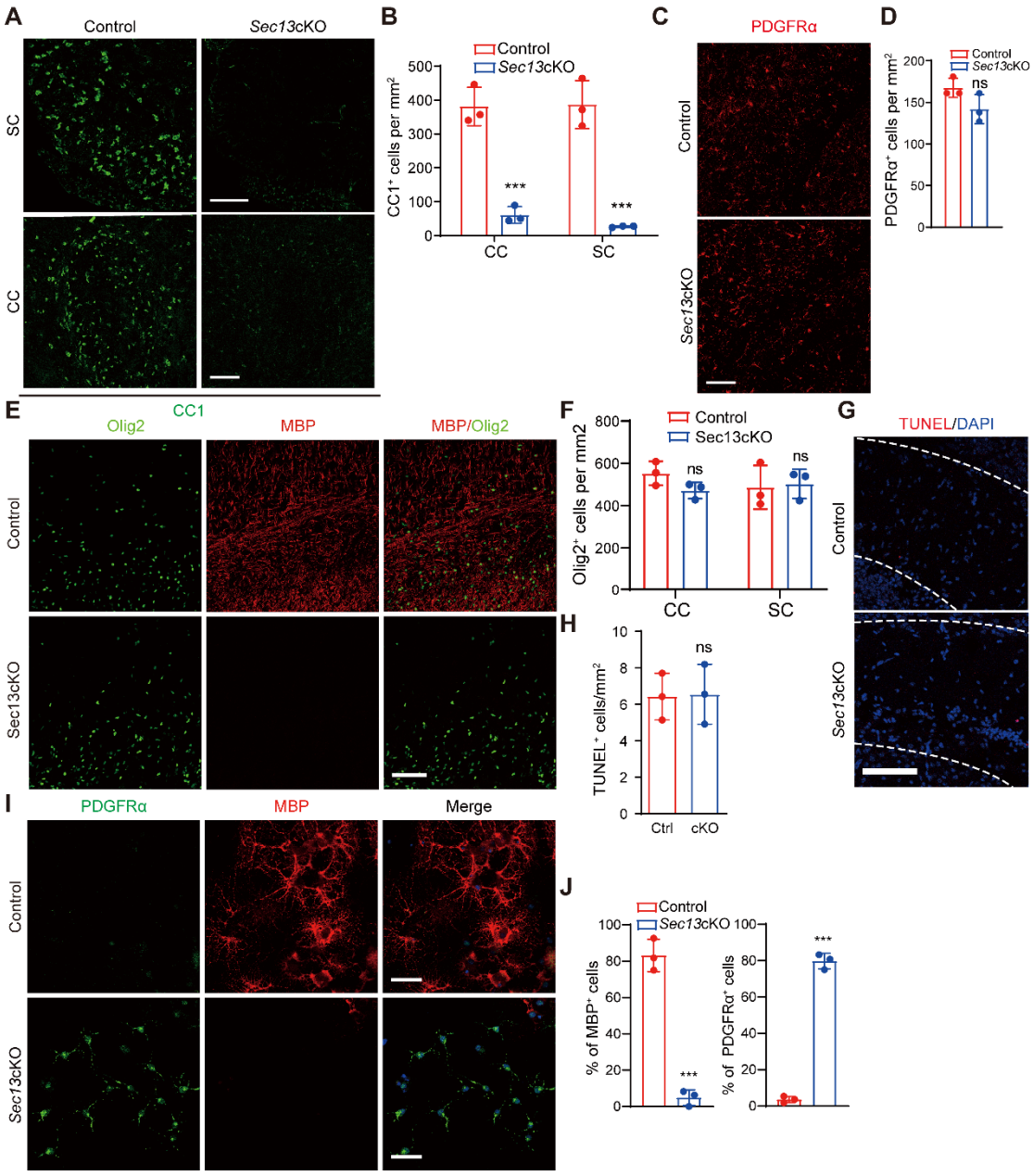
A
Control
Sec13cKO
SC
CC
B
Control
Sec13cKO
CC1+ cells per mm2
500
400
300
200
100
0
***
***
CC
SC
C
PDGFRα
Control
Sec13cKO
D
Control
Sec13cKO
PDGFRα+ cells per mm2
200
150
100
50
0
ns
E
CC1
Olig2
MBP
MBP/Olig2
Control
Sec13cKO
F
Control
Sec13cKO
Olig2+ cells per mm2
800
600
400
200
0
ns
ns
CC
SC
G
TUNEL/DAPI
Control
Sec13cKO
H
TUNEL+ cells/mm2
10
8
6
4
2
0
ns
Ctrl
cKO
I
PDGFRα
MBP
Merge
Control
Sec13cKO
J
Control
Sec13cKO
% of MBP+ cells
100
80
60
40
20
0
***
% of PDGFRα+ cells
100
80
60
40
20
0
***

921

922

Figure 4. Sec13 is required for OPC differentiation.

(A-B) Immunostaining (A) and quantification (B) of CC1 in the spinal cord (SC) and corpus callosum (CC) of control and *Sec13*cKO at P14 (n= 3 control and 3 mutant animals. Scale bars represent 100 μm.

(C-D) Immunostaining (C) and quantification (D) of PDGFRα in the corpus callosum of control and *Sec13*cKO at P14 (n= 3 control and 3 mutant animals). Scale bars represent 100 μm.

(E-F) Immunostaining (E) and quantification (F) of $Olig2^+$ cells in the corpus callosum (E) and spinal cord (SC) of control and *Sec13*cKO at P14 (n= 3 control and 3 mutant animals). Scale bars represent 100 μm.

(G-H) Representative images (G) and quantification (H) of TUNEL signal per field (1 mm^2) in the corpus callosum of control and *Sec13*cKO at P7 (n= 3 control and 3 mutant animals). Scale bars represent 100 μm.

(I) Immunolabeling of PDGFRα and MBP in control and *Sec13*cKO primary OPCs under differentiation conditions for 96h. Scale bars represent 50 μm.

(J) Quantification of MBP^+, $PDGFR\alpha^+$ cells from control and *Sec13*cKO under differentiation conditions for 96h (n= 3 control and 3 mutant animals). Data are represented mean ± SD; $^{***}P<0.001$, two-tailed unpaired Student's t test.

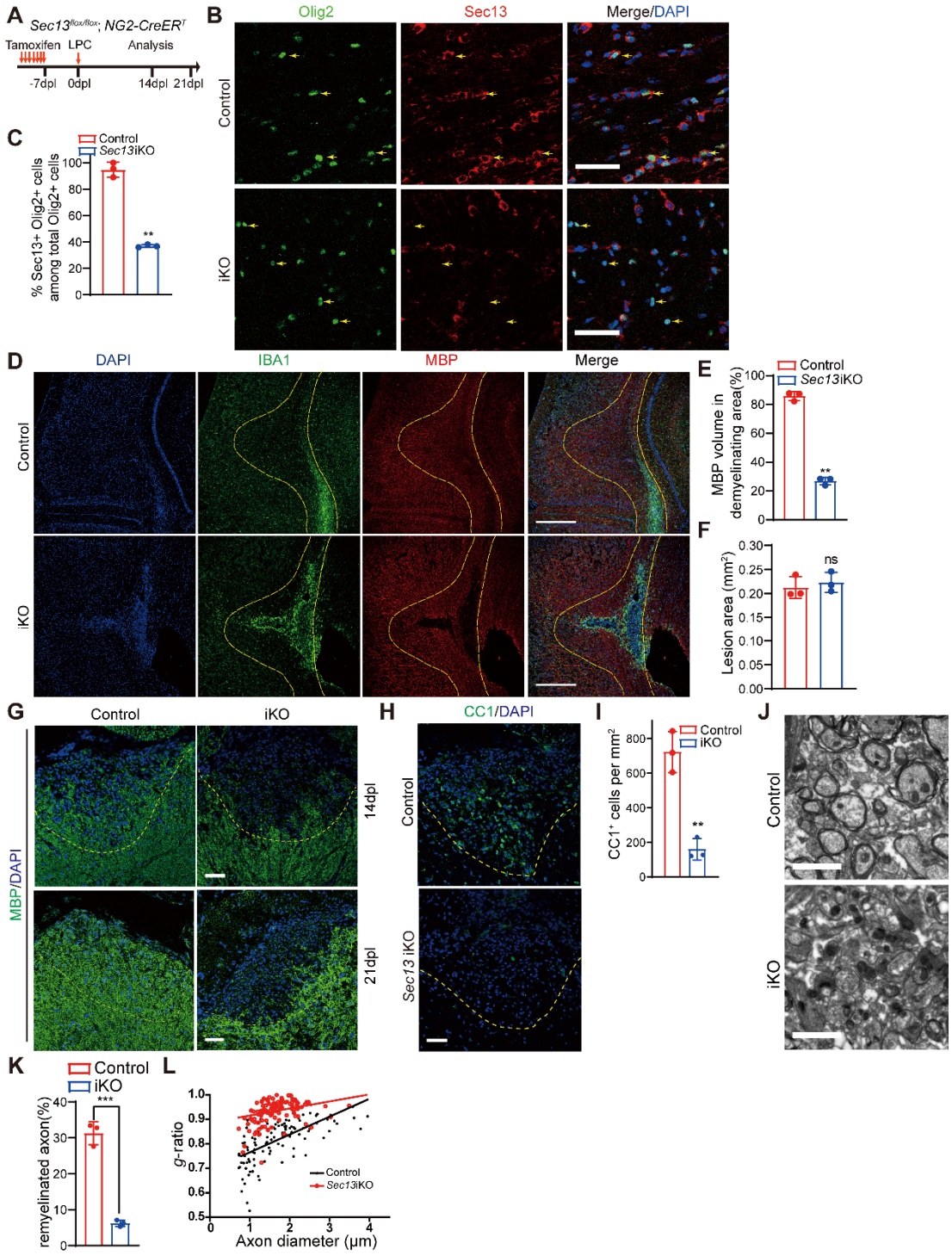
A
Sec13flox/flox; NG2-CreERT
Tamoxifen
LPC
Analysis
-7dpl
0dpl
14dpl
21dpl
B
Olig2
Sec13
Merge/DAPI
Control
iKO
C
Control
Sec13iKO
% Sec13+ Olig2+ cells among total Olig2+ cells
**
D
DAPI
IBA1
MBP
Merge
Control
iKO
E
Control
Sec13iKO
MBP volume in demyelinating area(%)
**
F
Lesion area (mm2)
ns
G
Control
iKO
MBP/DAPI
14dpl
21dpl
H
CC1/DAPI
Control
Sec13 iKO
I
Control
iKO
CC1+ cells per mm2
**
J
Control
iKO
K
Control
iKO
***
remyelinated axon(%)
L
g-ratio
Control
Sec13iKO
Axon diameter (μm)

941
942

Figure 5. Sec13 is critical for adult remyelination after demyelination.

(A) Diagram showing tamoxifen administration to 8-week-old control (*Sec13* $^{flox/flox}$) and *Sec13*iKO (*NG2-CreERT*: *Sec13* $^{flox/flox}$) mice followed by LPC injection seven days later.

(B) Immunostaining of Olig2 and Sec13 in the corpus callosum of control and *Sec13*iKO mice at 14 dpl. Arrowheads indicate the Olig2$^+$ cells. Scale bars represent 50 μm.

(C) Quantification of Sec13$^+$ Olig2$^+$ cells as a percentage of total Olig2$^+$ cells in the corpus callosum at 14 dpl (n= 3 control and 3 mutant animals).

(D) Immunostaining of IBA1 and MBP in corpus callosum lesions of control and *Sec13* iKO mice at 14 dpl. Scale bars represent 200 μm.

(E-F) Quantification of MBP$^+$ volume (E) and lesion area (F) in corpus callosum lesions of control and *Sec13*iKO mice at 14 dpl (n= 3 control and 3 mutant animals).

(G) Immunostaining of MBP in spinal cord lesions of control and *Sec13*iKO mice at 14 and 21 dpl. Scale bars represent 50 μm.

(H and I) Immunostaining (H) and quantification (I) of CC1$^+$ cells in spinal cord lesions of control and *Sec13*iKO mice at 14 dpl (n= 3 control and 3 mutant animals). Scale bars represent 50 μm.

(J) Electron microscopy of LPC lesion from control and *Sec13*iKO spinal cord at 14 dpl. Scale bars represent 2 μm.

(K) Quantification of remyelinated axons in LPC-induced lesion of control and *Sec13*iKO spinal cord at 14 dpl (n= 3 control and 3 mutant animals).

(L) The myelin *g*-ratio in LPC-induced lesions of control and *Sec13*iKO spinal cord at 14 dpl. Data are represented mean ± SD; $^{**}P<0.01$, $^{***}P<0.001$, two-tailed unpaired Student's t test.

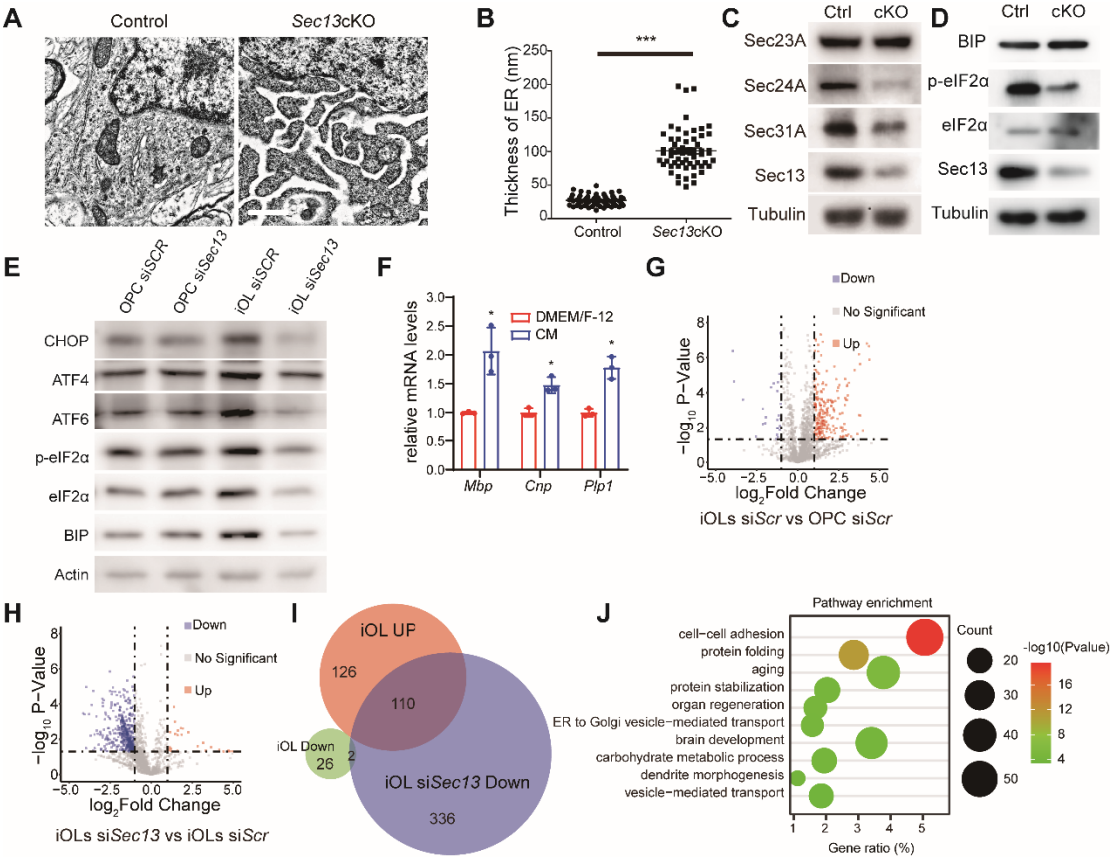
A
Control
Sec13cKO
B
Thickness of ER (nm)
250
200
150
100
50
0
***
Control
Sec13cKO
C
Ctrl
cKO
Sec23A
Sec24A
Sec31A
Sec13
Tubulin
D
Ctrl
cKO
BIP
p-eIF2α
eIF2α
Sec13
Tubulin
E
OPC siSCR
OPC siSec13
iOL siSCR
iOL siSec13
CHOP
ATF4
ATF6
p-eIF2α
eIF2α
BIP
Actin
F
relative mRNA levels
DMEM/F-12
CM
Mbp
Cnp
Plp1
G
Down
No Significant
Up
P-Value
log2Fold Change
iOLs siScr vs OPC siScr
H
Down
No Significant
Up
P-Value
log2Fold Change
iOLs siSec13 vs iOLs siScr
I
iOL UP
126
110
iOL Down
26
2
iOL siSec13 Down
336
J
Pathway enrichment
cell−cell adhesion
protein folding
aging
protein stabilization
organ regeneration
ER to Golgi vesicle−mediated transport
brain development
carbohydrate metabolic process
dendrite morphogenesis
vesicle−mediated transport
Gene ratio (%)
Count
-log10(Pvalue)

Figure 6. Sec13 regulates oligodendrocyte secretome.

(A) Electron microscopy analysis of the ER structure in spinal cords of control and *Sec13*cKO at P7. Scale bars represent 1 μm.

(B) Quantification of ER thickness in spinal cords of control and *Sec13*cKO at P7 (n=3 independent experiments).

(C-D) Immunoblotting of indicated proteins in primary control and *Sec13*cKO OPCs.

(E) Immunoblotting of indicated proteins in primary rat OPCs or differentiating immature oligodendrocytes following treatment with scrambled or *Sec13* siRNAs, respectively.

(F) Real-time PCR analysis of myelination-associated genes in primary rat OPCs under differentiation conditions following treatments with DMEM/F-12 or CM (n=3 independent experiments).

(G) Volcano plot showing differential protein abundance (highlighted in color; fold change>2; P-value<0.05) in the conditioned media of primary rat differentiating immature oligodendrocytes relative to OPC.

(H) Volcano plot showing differential protein abundance (highlighted in color; fold change>2; P-value<0.05) in the conditioned media of primary rat differentiating immature oligodendrocytes treated with *Sec13* siRNA relative to *scrambled* siRNA.

(I) Venn diagram showing the overlap between differentially secreted factors upon OPC differentiation and knockdown of Sec13 in differentiating immature oligodendrocytes.

(J) GO functional categories analysis of the proteins with reduced secretion after knockdown of Sec13. Data represent mean ± SD; $^{*}P<0.05$, $^{***}P<0.001$, two-tailed unpaired Student's *t* test.

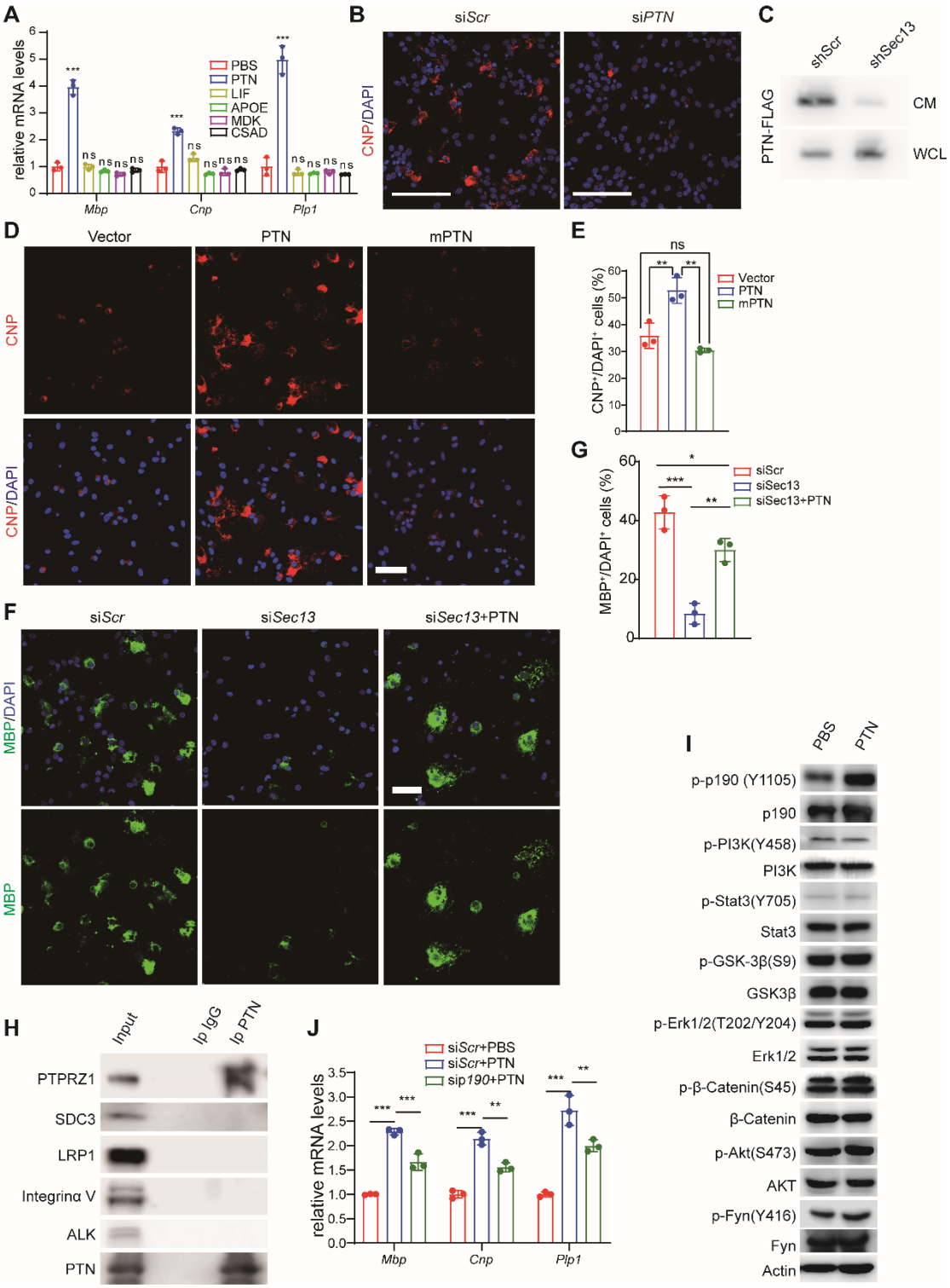
A
relative mRNA levels
PBS
PTN
LIF
APOE
MDK
CSAD
Mbp
Cnp
Plp1
B
siScr
siPTN
CNP/DAPI
C
shScr
shSec13
PTN-FLAG
CM
WCL
D
Vector
PTN
mPTN
CNP
CNP/DAPI
E
CNP+/DAPI+ cells (%)
ns
Vector
PTN
mPTN
G
MBP+/DAPI+ cells (%)
siScr
siSec13
siSec13+PTN
F
siScr
siSec13
siSec13+PTN
MBP/DAPI
MBP
I
PBS
PTN
p-p190 (Y1105)
p190
p-PI3K(Y458)
PI3K
p-Stat3(Y705)
Stat3
p-GSK-3β(S9)
GSK3β
p-Erk1/2(T202/Y204)
Erk1/2
p-β-Catenin(S45)
β-Catenin
p-Akt(S473)
AKT
p-Fyn(Y416)
Fyn
Actin
H
Input
Ip IgG
Ip PTN
PTPRZ1
SDC3
LRP1
Integrinα V
ALK
PTN
J
siScr+PBS
siScr+PTN
sip190+PTN
relative mRNA levels
Mbp
Cnp
Plp1

Figure 7. PTN promotes oligodendrocyte differentiation via autocrine signaling.
(A) Real-time PCR analysis of myelination-associated genes in primary rat OPCs under differentiation conditions without T3, but in the presence or absence of indicated recombinant factors (PTN, 100nM; LIF, 50ng/μL; APOE, 10μg/μL; MDK, 100nM; CSAD, 1.3ng/μL) (n=3 independent experiments).
(B) Immunolabeling of CNP in primary rat OPCs under differentiation conditions for 72hours following treatments with scrambled or *PTN* siRNAs. Scale bars represent 100 μm. Scr, scrambled.
(C) Immunoblotting of transfected PTN-FLAG in culture medium (upper, CM) and cellular lysate (lower, WCL=whole cell lysate) from Oli-neu cells transduced with scrambled or *Sec13* shRNA.
(D-E) Immunostaining (D) and quantification (E) of CNP signals in primary rat OPCs under differentiation conditions following PTN or PTN mutant (L18&20R) overexpression (n=3 independent experiments). Scale bars represent 50 μm.
(F-G) Immunostaining (F) and quantification (G) of MBP signals in primary rat OPCs under differentiation conditions following treatment with scrambled or *Sec13* siRNAs and recombinant PTN protein, respectively (n=3 independent experiments). Scale bars represent 50 μm.
(H) Co-immunoprecipitation of endogenous indicated factors with PTN in primary rat differentiating immature oligodendrocytes.
(I) Immunoblotting of indicated proteins in primary rat differentiating immature oligodendrocytes following treatment with recombinant PTN for 1h.
(J) Real-time PCR analysis of myelination-associated genes in primary rat OPCs under differentiation conditions following treatment with scrambled or *p190* siRNAs and recombinant PTN protein, respectively (n=3 independent experiments). Data are represented mean ± SD and were analyzed by 1-way ANOVA with Tukey's correction for multiple comparisons. *P<0.05, **P<0.01, ***P<0.001.

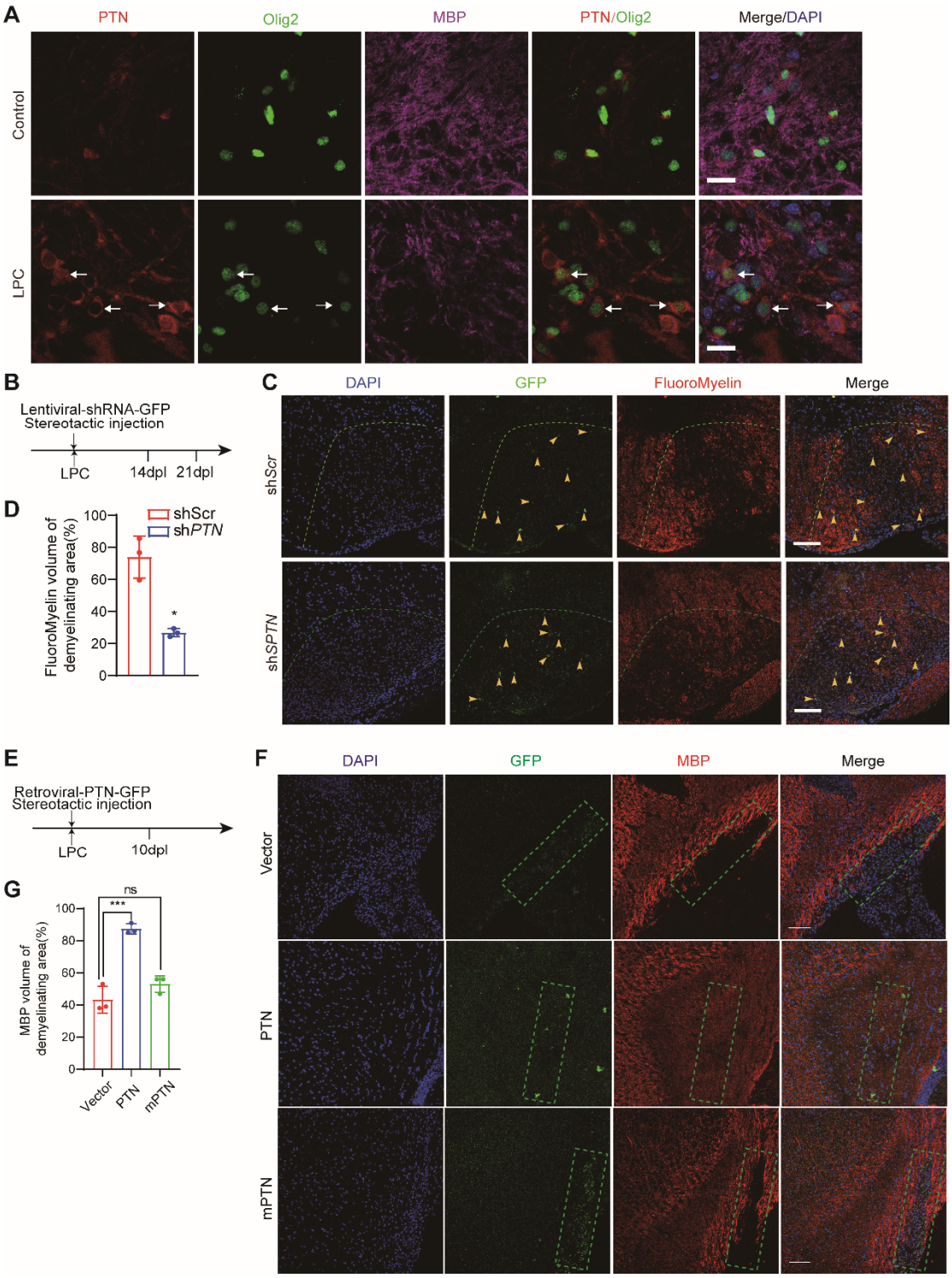
A
PTN
Olig2
MBP
PTN/Olig2
Merge/DAPI
Control
LPC
B
Lentiviral-shRNA-GFP
Stereotactic injection
LPC
14dpl
21dpl
C
DAPI
GFP
FluoroMyelin
Merge
shScr
shSPTN
D
FluoroMyelin volume of demyelinating area(%)
shScr
shPTN
E
Retroviral-PTN-GFP
Stereotactic injection
LPC
10dpl
F
DAPI
GFP
MBP
Merge
Vector
PTN
mPTN
G
MBP volume of demyelinating area(%)
ns
***
Vector
PTN
mPTN

Figure 8. PTN accelerate remyelination after demyelinating injury.

(A) Immunostaining of PTN, Olig2 and MBP at 7 dpl in spinal cord from non-lesion control and LPC lesion mice. Arrows indicate $PTN^+/Olig2^+$ cells. Scale bars represent 20 μm.

(B) Diagram showing injection of LPC and lentivirus expressing shRNA against PTN into spinal cord.

(C) Representative images of GFP and FluoroMyelin in spinal cord lesions of mice after injection of lentivirus expressing scrambled or *PTN* shRNA at 14 dpl. Arrowheads indicated GFP^+ cells. Scale bars represent 100 μm.

(D) Quantification of FluoroMyelin volume in spinal cord lesions of mice injected with lentivirus expressing scrambled or *PTN* shRNA at 14 dpl (n= 3 animals/treatment). Data are represented as mean ± SD; $^*P<0.05$, two-tailed unpaired Student's *t* test.

(E) Diagram showing injection of LPC and retrovirus expressing PTN or PTN mutant (L18&20R) into corpus callosum.

(F) Representative images of GFP and MBP in corpus callosum lesions of mice after injection of retrovirus expressing PTN or PTN mutant (L18&20R) at 10 dpl. Scale bars represent 100 μm.

(G) Quantification of MBP volume in corpus callosum lesions of mice after injection of retrovirus expressing PTN or PTN mutant (L18&20R) at 10 dpl (n= 3 animals/treatment).Data are represented mean ± SD and were analyzed by 1-way ANOVA with Tukey's correction for multiple comparisons. ***P<0.001.